12/8-5-92 DS (1)

PNL-8152
UC-602

Fifth In Situ Vitrification Engineering-Scale Test of Simulated INEL Buried Waste Sites

T. M. Bergsman
J. W. Shade
R. K. Farnsworth

June 1992

Prepared for the U.S. Department of Energy
under Contract DE-AC06-76RLO 1830

Pacific Northwest Laboratory
Operated for the U.S. Department of Energy
by Battelle Memorial Institute

Battelle

PNL-8152

DISCLAIMER

PACIFIC NORTHWEST LABORATORY
operated by
BATTELLE MEMORIAL INSTITUTE
for the
UNITED STATES DEPARTMENT OF ENERGY
under Contract DE-AC06-76RLO 1830

Printed in the United States of America

Available to DOE and DOE contractors from the Office of Scientific and Technical Information, P.O. Box 62, Oak Ridge, TN 37831; prices available from (615) 576-8401. FTS 626-8401.

Available to the public from the National Technical Information Service, U.S. Department of Commerce, 5285 Port Royal Rd., Springfield, VA 22161.

PNL--8152

DE92 017951

FIFTH IN SITU VITRIFICATION ENGINEERING-SCALE TEST OF SIMULATED INEL BURIED WASTE SITES

T. M. Bergsman
J. W. Shade
R. K. Farnsworth[a]

June 1992

Prepared for
the U.S. Department of Energy
under Contract DE-AC06-76RLO 1830

Pacific Northwest Laboratory
Richland, Washington 99352

(a) EG&G Idaho, Inc.
Idaho Falls, Idaho

SUMMARY

In September 1990, an engineering-scale in situ vitrification (ISV) test was conducted on sealed canisters containing a combined mixture of buried waste materials expected to be present at the Idaho National Engineering Laboratory (INEL) Subsurface Disposal Area (SDA). The test was part of a Pacific Northwest Laboratory (PNL)[a] program to assist INEL in treatability studies of the potential application of ISV to mixed transuranic wastes at the INEL SDA.[b] The purpose of this test was to determine the effect of a close-packed layer of sealed containers on ISV processing performance. Specific objectives included determining (1) the effect of releases from sealed containers on hood plenum pressure and temperature, (2) the release pressure and temperatures of the sealed canisters, (3) the relationships between canister depressurization and melt encapsulation, (4) the resulting glass and soil quality, (5) the potential effects of thermal transport due to a canister layer, (6) the effects on particle entrainment of differing angles of approach for the ISV melt front, and (7) the effects of these canisters on the volatilization of volatile and semivolatile contaminants into the hood plenum. Two hundred test canisters were arranged in a layer extending outside of the melt zone on one side. The test canisters contained a base sludge that was a combined mixture of potential waste types at the INEL SDA. In addition, the sludge composition was slightly varied among the canisters to determine the effect of canister location (relative to the ISV melt front) on off gas releases and particulate entrainment from the sealed containers. The four sludge compositions contained different hazardous volatiles and semivolatiles (carbon tetrachloride, trichloroethane, trichloroethylene, tetrachloroethylene and mercury), and lanthanide tracers.

(a) Operated for the U.S. Department of Energy by Battelle Memorial Institute under Contract DE-AC06-76RLO 1830.

(b) The current focus of the ISV Integrated Program is to resolve technical issues associated with contaminated soil applications and to implement the technology for soils. Development of ISV for advanced applications, such as buried waste, is on hold pending resolution of the contaminated soils technical issues.

Out of the 200 cans used in the test, 87 were either totally or partially incorporated into the melt. An additional 9 cans showed visual evidence of rapid depressurization. Of this total (96), 51 ruptured with releases significant enough to positively pressurize the engineering system container. Data from these pressurization events indicate that the rupturing was caused by an energetic reaction between organics and nitrates contained in the base sludge. This reaction was likely initiated by high pressure in the test canister coupled with the approach of the high-temperature melt front. This type of reaction is unlikely in the INEL SDA since organics and nitrates are packaged in separate containers. In addition, the tight seal on the canisters resulted in pressures that are much higher than would be expected for a full-scale drum. Therefore, the results of this test are unlikely to be representative of a full-scale application.

The vitrified glass product passed the Toxicity Characteristic Leach Procedure (TCLP). Soil samples were also analyzed using TCLP. No soil sample contained hazardous levels of organics, and only one soil sample contained Hg above TCLP limits. This sample was below the canister layer at the 100°C isotherm. It is suspected that the Hg was transported to the 100°C isotherm on the canister side as a result of the force of the rupturing canisters and the increased permeability at the soil/canister interfaces. Essentially all of the lanthanide tracer in the canisters placed directly under the melt was encapsulated into the melt. The tracer placed in canisters toward which the melt front approached at an angle indicated the greatest entrainment into the off-gas system. A quantitative assessment of particulate entrainment could not be made, however, due to the loss of sample system isokineticity, which was caused by adjustments in the off-gas rate.

CONTENTS

FIGURES

TABLES

1.0 INTRODUCTION

In situ vitrification (ISV) is a hazardous waste remediation technology used to treat soils contaminated with a variety of hazardous organic, inorganic, or radioactive materials. ISV uses the principle of joule heating to melt contaminated soils, destroying organic compounds and assimilating metals and radioactive compounds into the melt. The process temperatures are in the range of 1600°C to 2000°C, which enables the molten zone to destroy the organic compounds through pyrolysis. At completion, the molten soil cools and solidifies to form a chemically inert glass and crystalline product.

The Environmental Restoration Program (ERP) established by EG&G Idaho, Inc. at the Idaho National Engineering Laboratory (INEL) is conducting a Remedial Investigation/Feasibility Study (RI/FS) for permanent disposal of INEL waste in compliance with the Comprehensive Environmental Response, Compensation, and Liability Act (CERCLA). As part of the RI/FS and in support of the Buried Waste Integrated Demonstration, an ISV scoping study on the treatability of mixed low-level and mixed transuranic-contaminated waste was performed to determine the applicability of ISV to remediation of waste at the INEL Subsurface Disposal Area (SDA). As part of this study, a series of engineering-scale tests was performed. This is the fifth engineering-scale test of this study (designated ES-INEL-5).

The primary objective of ES-INEL-5 was to evaluate the effect of a layer of containerized sludge (simulating Series 74 sludge from the Rocky Flats Plant) in INEL soil on containment of gas releases and transport of contaminants both subsurface and to the off-gas system. The data collected are intended to be used to determine the feasibility of conducting an ISV large-scale field test at Pit 9 of the INEL SDA. The test included 200 sealed carbon steel canisters, 5.5 oz in volume, that were arranged in a layer that extended beyond the melt zone. The simulated sludge contained a mixture of halogenated hydrocarbons (carbon tetrachloride [CCl_4], tetrachloroethylene [PCE], trichloroethane [TCA], trichloroethylene [TCE]), mercury (Hg), lanthanide tracers, and other components to simulate composite mixture of the

various Series 74 sludges in Pit 9 of the SDA. Specific questions and objectives addressed by this test are discussed in Section 4.0.

2.0 CONCLUSIONS

The fifth engineering-scale test on INEL soils was designed to evaluate the extent of possible effects from the vitrification of sealed containers. Two hundred test canisters were placed in a test layer that extended outside of the melt on one side. The canisters were divided into four different groups. One group was completely encapsulated by the melt. The second group was predominantly encapsulated, but these canisters were located outside the electrodes so the melt front approached them more from the side rather than from overhead. The third group was not encapsulated but was thermally affected by the melt. The final group was designed to be largely unaffected by the melt. Each group contained the same base sludge but different hazardous organics and lanthanide tracers. The base sludge was a combined mixture of the Series 74 sludge components expected in Pit 9 of the INEL SDA.

Seven test objectives were identified for ES-INEL-5. The conclusions drawn from the data relating to these objectives are given below.

How do the pressurized releases from sealed containers affect the off-gas composition, and how do the releases affect the pressure and temperature of the hood plenum?

Out of 200 cans used in the test, 87 were either totally or partially incorporated into the melt. An additional 9 cans showed visual evidence of rapid depresurization. Of this total (96), 51 ruptured with releases significant enough to positively pressurize the engineering system container. Data from these pressurization events indicate that the rupturing was caused by an energetic reaction between oils and nitrates contained in the base sludge. The temperature of the hood plenum was only slightly affected. The rupturing of the test canisters also produced NO_x releases to the off-gas system; however, 76% of the theoretical maximum NO_x was destroyed.

This type of reaction is unlikely in the INEL SDA since organics and nitrates are packaged in separate containers. In addition, the degrees of sealing, and resultant high pressures in the test canisters are much higher

than would be expected for a full-scale drum. Therefore, the results of this test are unlikely to be representative of a full-scale application. Nevertheless, the results may be useful in predicting the magnitude of a hood pressurization resulting from a specific canister depressurization.

What are the burst pressures of the carbon steel containers, and how do they relate to the temperatures inside the can and the temperature of the advancing melt front at the time of release?

Fifteen test canisters were internally monitored for temperature and pressure at various radial locations in the melt. Of these 15, only two burst and pressurized the hood. These two canisters burst at internal pressures in excess of 50 psig. Other test canisters, which did not rupture, also reached internal pressures in excess of 50 psig. However, for these other canisters, the pressures slowly decreased indicating leakage from the canister. The melt front temperature was monitored above three of the instrumented canisters, including the two that ruptured. For the canisters that ruptured, this melt front temperature was greater than 900°C while the canisters were still pressurized. For the canister that did not burst, the melt front temperature did not exceed 900°C until the canister had completely depressurized. Therefore, a combination of high pressure in the canister and high melt front temperature appears to be necessary to initiate the reaction that caused the cans to burst. Temperatures inside the canisters were relatively cool and constant (approximately 100° to 150°C) prior to depressurization and melt encapsulation. This indicates that volatilization and leakage from the canister were occurring, effectively cooling the canister.

What are the rates of canister depressurization and melt encapsulation, and the relationships between each rate?

Melt encapsulation (as measured by internal canister temperature) proceeded rapidly once the canisters depressurized. The canisters that depressurized more slowly (i.e., the ones where the pressure leaked off versus burst) were encapsulated more slowly. Volatilization of the components in the canisters appeared to provide a mechanism to cool the canisters and the melt front above them, delaying encapsulation. The temperatures in the canisters also showed an interesting spike at 700° to 800°C, followed by a cooling off

before rising again to the melt temperature. This spike was likely due to an endothermic reaction occurring prior to melt encapsulation (e.g., the release of chemically bound water).

What is the product quality of the vitrified block and surrounding soils resulting from ISV processing?

Samples of the glass block were analyzed using the Toxicity Characteristic Leach Procedure (TCLP) for the regulated metals. The TCLP results were several orders of magnitude below regulatory limits. Therefore, the resultant ISV waste form can be considered nonhazardous. This is consistent with previous product quality data on the ISV waste form.

Several soil samples were collected on either side of the vitrified block at the level of the canisters and directly beneath the block. The samples were analyzed using TCLP (for Hg) and TCLP-Zero Headspace Extraction (TCLP-ZHE) procedures (for CCl_4, TCA, TCE, and PCE). In addition, the samples were analyzed for Hg using inductively coupled plasma/mass spectroscopy (ICP/MS) and volatile organics (for CCl_4, TCA, TCE, PCE) using gas chromatography/mass spectrometry (GC/MS).

None of the samples contained hazardous levels of organics, and there was no measurable CCl_4 in any sample. (CCl_4 was contained in the canisters that were completely encapsulated by the melt. By design, several of the canisters were not completely encapsulated.) No measurable organics were found at temperatures below the 350°C isotherm. These results for volatile organics are consistent with the results found in ES-INEL-4 (Shade et al. 1991) that indicated the volatile organics were in large part either transported to the off-gas system or destroyed.

In one instance, it appeared that the TCLP levels for Hg were exceeded in the soils at the 100°C isotherm on the canister side. The transport mechanism to this location was likely not a thermal one since the condensation point of Hg is approximately 350°C and the vapor pressure for Hg is only 0.27-mm Hg at 100°C. The more likely mechanism was the gas entrainment of particulate or Hg vapor. The canisters ruptured with significant force (because of the reaction of organics and nitrates), increasing the likelihood of this entrainment. In

addition, the canisters were arranged in line such that the gas entrainment would be enhanced. This combination of factors is significantly beyond what would be expected in the SDA.

Does the presence of a sealed drum layer enhance the thermal transport of organics and semivolatile inorganics away from the advancing melt front?

A comparison of the results between the soil side of the melt and the canister side of the melt indicated that the canister layer may actually improve the removal of organics. This could be due to the greater permeability of the region around the canisters allowing the organics to more easily be transported toward the melt front to be destroyed and removed. The amount of Hg, on the other hand, was greater on the canister side. As discussed above, the transport of Hg was likely not just a thermal one, and the greater permeability on the can side probably allowed greater gas entrainment of particulate.

How is the entrainment of nonvolatile particulates related to the approach angle of the advancing melt front?

As might be expected, the entrainment of nonvolatile particulates appeared to be greatest from the canisters located at the edge of the melt (the melt front approached from the side.) In addition, those canisters that ruptured due to the thermal effects of the melt also showed greater entrainment. These data, however, are somewhat compromised since the off-gas rate was changed during the test due to the pressurizations. Therefore, the sampling was not always isokinetic.

Analysis of the glass block indicates that essentially all of the lanthanide tracer in the canisters placed directly under the melt was encapsulated into the melt. The tracer placed in canisters for which the melt front approached at an angle was not completely encapsulated. However, this is not surprising since the canisters themselves were not fully incorporated by the melt.

Does the pressurized release of gas-generating materials (such as water, volatile organics, and nitrates) from sealed carbon steel containers increase the volatility and entrainment of hazardous or radioactive materials to the

off-gas system? Would this result in incomplete organic combustion above the melt?

Insufficient data were gathered to answer this question. The off gas was sampled using a SUMA canister that collected a small amount of gas at a constant rate throughout the duration of the test. During pressurizations, the off-gas flow rate was increased, compromising the usefulness of these data. A grab sample was taken during a pressurization, and another sample was taken during posttest cool down, but a quantitative comparison of the data could not be made. Ideally, any further testing to address this issue should be performed using an on-line analyzer or a greater series of samples.

3.0 TEST DESCRIPTION

3.1 TEST COMPONENTS AND CONFIGURATION

The ES-INEL-5 test configuration and sludge composition were designed to evaluate conditions in Pit 9 of the INEL SDA. The test sludge composition was based on a composite simulation of the five Series 74 sludges which are expected to be the predominant waste in Pit 9 (estimated per Wierman [1990]). The composition was determined by estimating the overall amounts of particular components relative to the total in the pit. These estimates were used to determine the various percentages in the base sludge composition.[(a)] Different hazardous volatile organics and rare earth oxides were then added as tracers to this base sludge composition to create four different test series sludges (lettered A through D). The Series A sludge also contained mercury, which was added as mercuric oxide to obtain a more homogeneous distribution of mercury in the sludge. The composition of the four different test series sludges is given in Table 3.1.

The four sludges were placed in 200 sealed canisters that were arranged in a continuous layer within the soil but extending outside of the melt zone. The Series A canisters were placed in the melt zone between the electrodes, and the Series D canisters were placed outside the melt zone at the extremity of the canister layer. Part of Series B and C were between Series A and D. The use of different rare earth tracers in each of the series was intended to indicate the effect of the melt front approach angle on enhanced off-gas particulate entrainment and to indicate the extent of canister breaching beyond the melt area. The use of TCA, TCE, and CCl_4 in three of the four sludges was intended to provide an indication of organic transport, both to the off gas and away from the advancing melt front, without significantly changing the volatile and combustible nature of the sludge. The elimination

---

(a) Although the base composition represents an average of the total sludges found in Pit 9 of the SDA, it is not representative of individual sludges in individual containers. In the SDA, each of the five Series 74 sludges are buried in separate containers.

TABLE 3.1. Simulated Sludge Compositions for ES-INEL-5, wt%

Sludge Component	Series A	Series B	Series C	Series D
Water	17.9	19.1	18.8	21.3
Sodium nitrate	16.5	17.6	17.4	19.7
Potassium nitrate	11.0	11.7	11.6	13.1
Calcium silicate	8.42	8.97	8.84	10.0
UnoCal Soluble 10 Oil	5.73	6.10	6.01	6.82
Texaco Regal Oil-R&O 68	5.21	5.54	5.46	6.19
Portland cement	3.83	4.08	4.02	4.56
$Fe_2(SO_4)_3$	2.56	2.73	2.69	3.05
$CaCl_2$	2.56	2.73	2.69	3.05
$MgSO_4$	2.56	2.73	2.69	3.05
Al_2O_3	2.56	2.73	2.69	3.05
SiO_2	2.56	2.73	2.69	3.05
Acetic acid	0.77	0.83	0.81	0.92
EDTA[(a)]	0.67	0.71	0.70	0.79
Alcohol (i-Propanol)	0.59	0.63	0.62	0.70
CCl_4	11.9	--	--	--
PCE	2.32	--	--	--
1,1,1-TCA	--	10.6	--	--
TCE	--	--	11.8	--
Mercuric oxide	1.81	--	--	--
Dy_2O_3	0.499	--	--	--
Yb_2O_3	--	0.528	--	--
Nd_2O_3	--	--	0.533	--
CeO_2	--	--	--	0.636
Total	100.0	100.0	100.0	100.0

(a) EDTA = ethylenediaminetetraacetic acid.

of mercuric oxide and PCE from the Series B and C sludges, and all of the hazardous materials from the Series D sludges, was expected to provide a better means of evaluating thermal transport away from the melt front into materials free from hazardous constituents.

A sufficient amount of sludge was prepared to fill about 200 small (5.5-oz) carbon steel containers with 245 g of sludge each. The containers were approximately 5 cm (2 in.) dia x 7.5 cm (3 in.) tall. After filling with

the appropriate sludge composition, each container was sealed with a crimp-on lid using standard canning methods. They were placed on their sides in a single layer at a depth of 30 to 35 cm (12 to 14 in.) to simulate a scaled-down layer geometrically (based on electrode spacing) equivalent to a 55-gal drum layer at a depth of 3.5 to 4.0 m (11.5 to 13.5 ft).

The sealed containers were arranged in the test soil such that 1/4 of the container layer had a total radius from the center of at least 76 cm (30 in.), while the other 3/4 had a total radius from center of only 30 cm (12 in.) (Figure 3.1). The 30-cm (12-in.) radius was expected to represent the maximum horizontal growth of the melt zone; the 76-cm (30-in.) radius was expected to represent the maximum expected radius of the 100°C isotherm surrounding the vitrified block. To increase the potential for enhanced material transport through the drum layer, the containers were placed in the same horizontal orientation for all but some corners of the layer.

The electrode spacing used for the test was a 30-cm (12 in.) square arrangement. The number of containers used in each series, their trace element content, and their geometric arrangement with respect to the electrodes in the test are summarized below and shown in Figure 3.1, both in plan view and in cross section.

- Series A canisters - Twenty-four canisters were placed within the cross-sectional area of the electrodes. These canisters contained Hg, CCl_4, PCE, and dysprosium (III) oxide as the lanthanide tracer. These canisters were completely vitrified and encapsulated by the melt. The advancing melt front approached directly from above the containers.

- Series B canisters - A total of 64 Series B canisters containing TCA and ytterbium (III) oxide tracer were placed such that they completely surrounded the Series A canisters. The minimum radius of the outer edge of these canisters (from the center of the melt) was 30 cm (12 in.). These canister were expected to come in contact with the advancing melt front and be nearly or totally encapsulated by the melt. The advancing melt was expected to approach these containers at some angle between 0° and 90° from the vertical.

- Series C canisters - There were 48 Series C canisters containing TCE and neodymium (III) oxide tracer surrounding just over 1/4 of the Series B and Series A containers. The minimum radius of the outer edge of these containers was 53 cm (21 in.). It was not

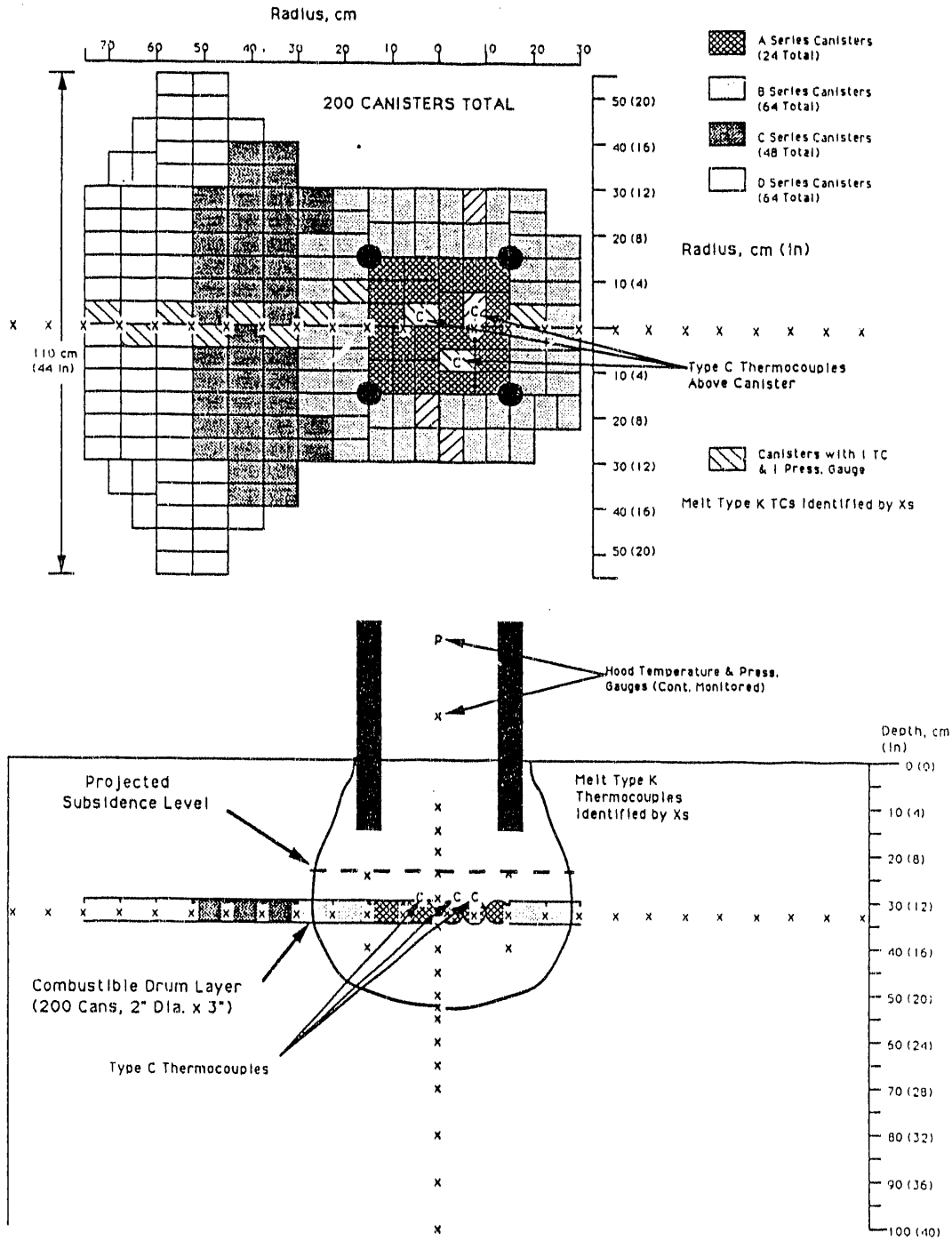

FIGURE 3.1. ES-INEL-5 Test Configuration

expected that these containers would be encapsulated by the melt, but there was a possibility that some of them would be breached during processing.

- Series D canisters - There were 64 Series D canisters containing cerium (IV) oxide placed outside the Series C, B, and A canisters. The minimum radius of the outer edge of these canisters is 76 cm (30 in.). It was not expected that these canisters would be encapsulated and the potential for breaching was considered to be negligible.

To determine how the approaching melt front would affect the canister burst pressure and temperature and the rates of depressurization and encapsulation, selected canisters from each sludge layer were internally monitored for temperature and pressure using Type K thermocouples and appropriately sized pressure transducers. Because the rate of depressurization was expected to be relatively fast, each thermocouple and pressure transducer in the selected canisters were monitored at rates of 15 s and 0.5 s, respectively, using a computer system. As shown in Figures 3.1 and 3.2, the total number of canisters selected for internal monitoring was 15 (lettered A through O on Figure 3.2), 3 canisters from Series A, 6 canisters from Series B, 3 canisters from Series C, and 3 canisters from Series D.

In addition to these thermocouples and pressure transducers in the cans, Type K thermocouples were used to monitor the melt and soil isotherm growth both horizontally and vertically downward. The Type K thermocouples in the center of the melt were placed starting at 10 cm (4 in.) below the soil surface and at 2.5-cm and 5-cm (1-in. and 2-in.) intervals as shown in Figure 3.1. The test used two sets of lateral thermocouples to measure horizontal melt growth, with one set located in the sealed container layer, and the other set located in the soil layer on the opposite side of the melt. As indicated in Figure 3.1, both edge thermocouple sets were at a depth of 33 cm (13 in.) and started at 7.6 cm (3 in.) off the melt center and proceeded outward at 7.6-cm (3-in.) intervals. Additional Type K thermocouples were placed at 25-cm (10-in.) and 40-cm (16-in.) depths, 15 cm (6 in.) off center, on both the canister side and the soil side.

Three high-temperature Type C thermocouples were used to monitor actual melt temperatures during the test. These were located at a 30-cm (12-in.) depth, directly above the three Series A canisters being internally monitored

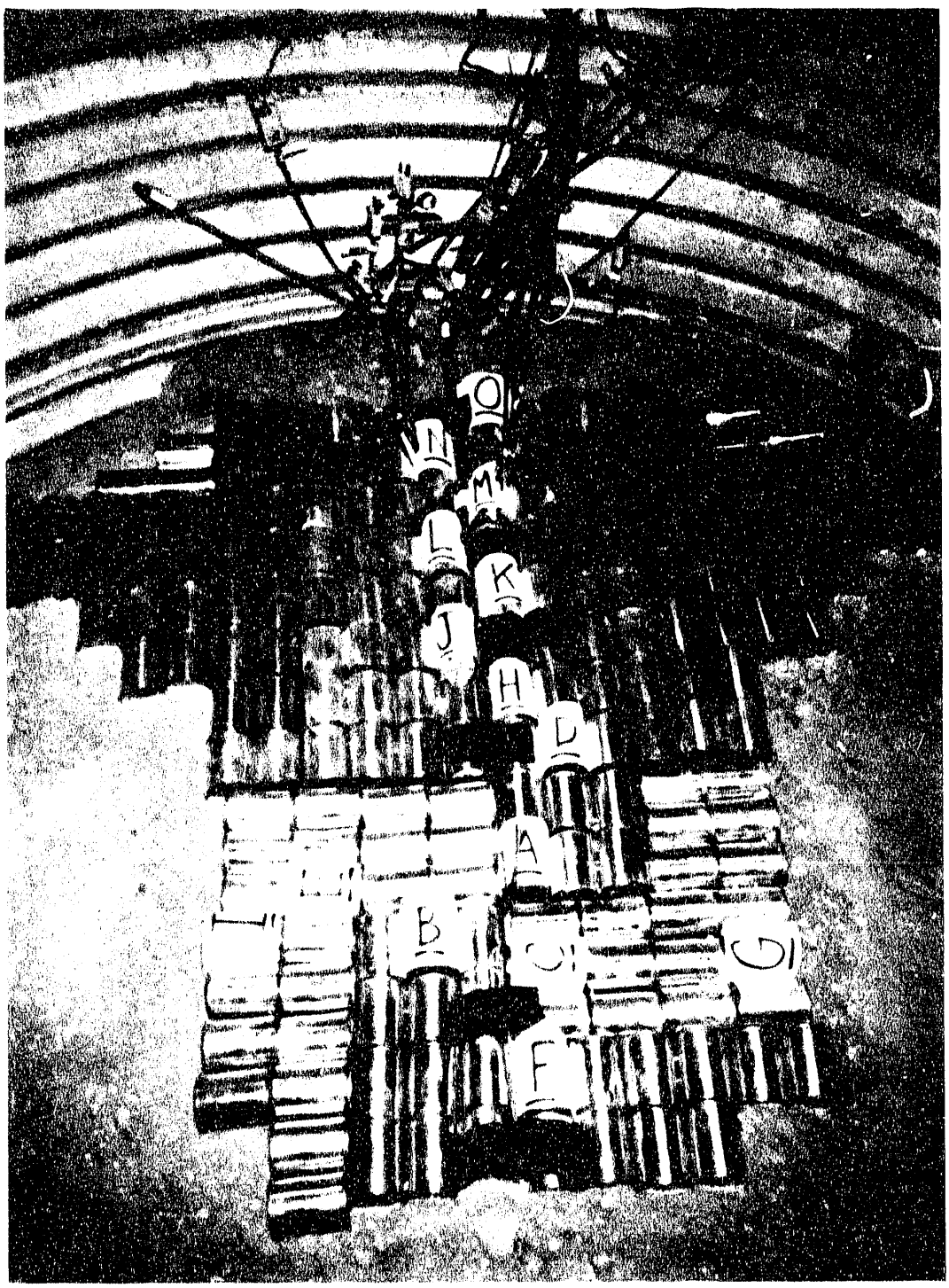

FIGURE 3.2. ES-INEL-5 Canister Layout (instrumented canisters are lettered A through O)

for temperature and pressure (Figure 3.1). These Type C thermocouples were also used to determine the temperature above the instrumented canisters at the time each canister released its contents.

The four test electrodes were fabricated from three sections of uncoated graphite, 5 cm (2 in.) dia x 46 cm (18 in.) long. The electrodes were initially inserted in the upper soil to a 15-cm (6-in.) depth, and were spaced in a 30.5 cm x 30.5 cm (12 in. x 12 in.) square array as shown in Figure 3.1. A graphite starter path of a 65:35 mixture of graphite and frit was laid in a criss-crossed square arrangement such that a linear starter path was between each electrode. The cross-sectional area of the starter path was 2.5 cm x 2.5 cm (1 in. x 1 in.).

The zone to be vitrified was covered with sand and at least 5 cm (2 in.) of blanket insulation, leaving a 1.25-cm (0.5-in.) gap around each electrode in the insulation for venting. The insulation was intended to help promote subsidence of the molten glass surface and improve efficiency of the melting operation.

3.2 TEST HARDWARE AND OFF-GAS SAMPLING SYSTEM

The test was performed in the ISV engineering-scale processing container. The container measures 1.8 m (6 ft) dia x 2.4 m (8 ft) tall. The initial hood plenum height was 63.5 cm (25 in.). The initial off-gas rate was 637 L/min (22.5 scfm). This rate was chosen to simulate the expected off-gas residence time for a large-scale ISV field test (approximately 2.5 min).

Off gas from the vitrification zone was sampled continuously during the test. A fraction (26.9 L/min) of the total off-gas flow was drawn into a Modified Method 5 (MM5) sampling train containing a filter, two impingers filled with 100 mL of 3% hydrogen peroxide (H_2O_2), one empty impinger, and one impinger filled with silica gel (see Figure 3.3). This train was designed to capture mercury, nitric oxides, sulfuric oxides, and rare earth oxides that were either volatilized or entrained to the ISV system off gas and drawn into the sampling system. The system was set up to operate isokinetically at the initial off-gas flow rate of 637 L/min (22.5 scfm) for the test. Because of pressurizations, however, the off-gas flow rate was increased periodically

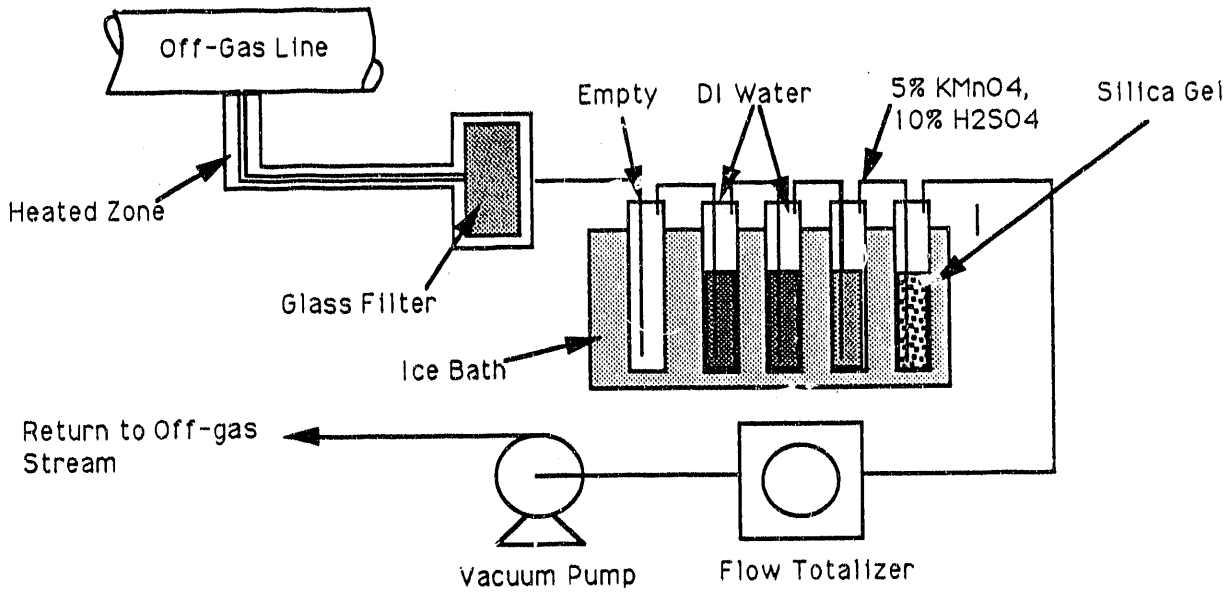

FIGURE 3.3. Modified MM5 Sampling Train

during the test. Therefore, the data from this system were not isokinetic and any conclusions drawn from these data must be used with caution.

A second sampling train was used to sample organics. This sample train, shown in Figure 3.4, was prepared in accordance with Compendium Method TO-14. This sampling method was different from the method used in ES-INEL-4, which used small sorbent resin tubes. That test, however, showed significant saturation and breakthrough of the volatile organic materials.

The ES-MEL-5 sampling system involved sample collection via an evacuated SUMA canister that is designed to collect uniformly integrated air samples over a predetermined time period. These SUMA canisters are electropolished stainless steel canisters, with the interior surface of the canisters passivated using the Molectrics SUMA process. The sampling apparatus included a leak-free metal bellows pump, a mechanical critical orifice flow regulator, and a mechanical compensating flow restrictive device. A Teflon sample line was inserted into the port to pull a gas sample through the flow controller and into the canister. As discussed above, the off-gas flow rates were changed during the test due to pressurizations. Therefore, the ratio of the

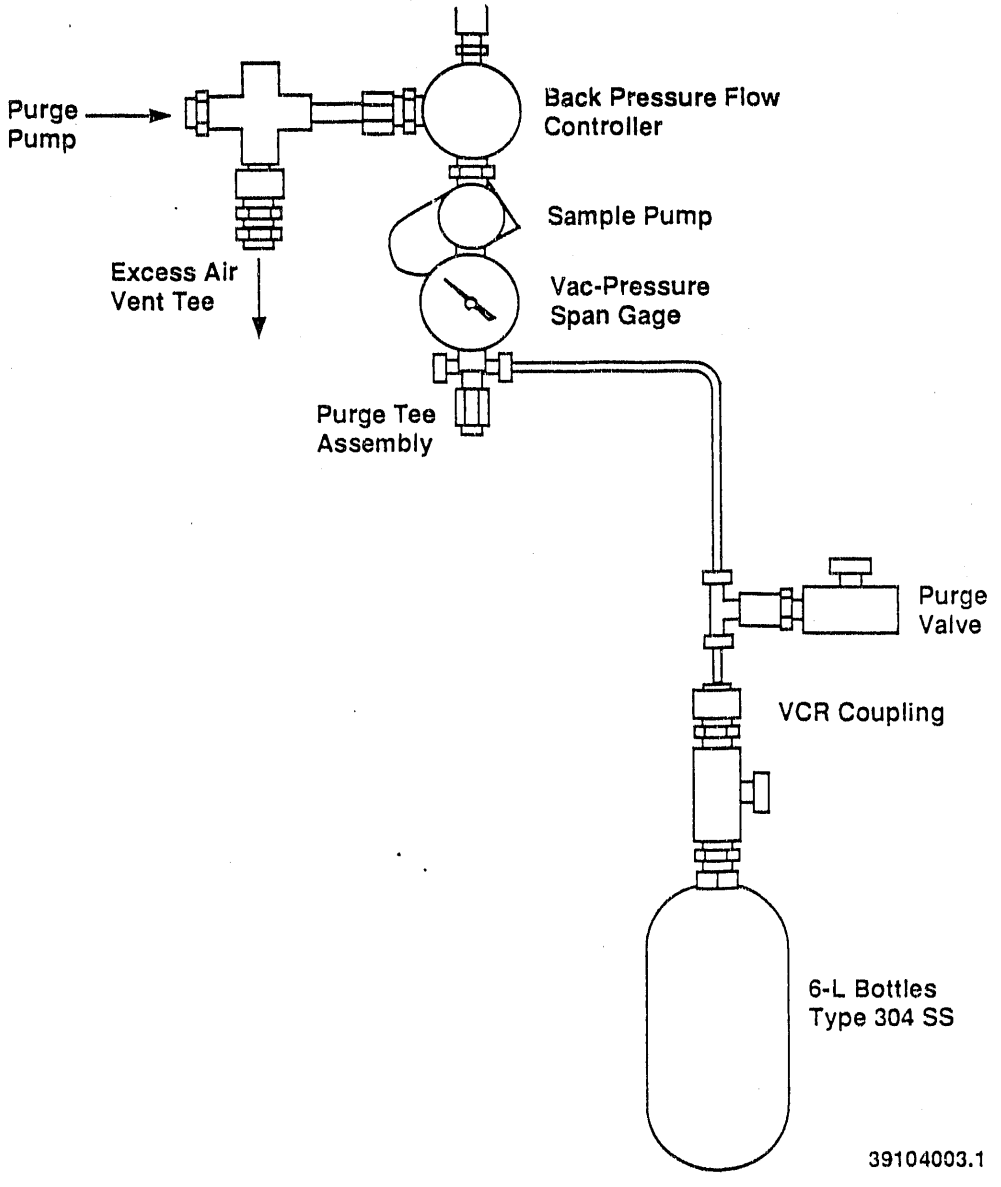

FIGURE 3.4. TO-14 Sample System Schematic for ES-INEL-5

flow into the SUMA canister to the total flow varied during the test. Again, any conclusions drawn from these data must be used with caution.

Specific data from the test were recorded on the data acquisition system that was developed by Battelle in National Instrument's LabVIEW© 2 to run on a Macintosh IIX equipped with three National Instrument LAB-MIO16 16-channel

Analog Input interface boards. The system allows the operator to select separate scanning rates for each of the three analog input boards.

For ES-INEL-5, the first input board was scanned at a rate of once every 0.5 s. The 16 channels of information included the pressures of Cans A through O and the hood pressure. The second board was scanned at a rate of once every 15 s, and the 16 channels of information contained the internal temperatures of Cans A through O (Type K thermocouples) and the hood temperature. The third board was scanned at a rate of once every 5 s and contained the melt front temperatures of Cans A, B, and C (Type C thermocouples), the concentration of NO_x in the off gas, A-phase and B-phase volts, amps, and power levels. For this third board, only the Type C thermocouple readings and the NO_x concentration readings were assumed valid.

3.3 PRETEST SAMPLING

Pretest sample components included the pretest INEL soil, samples of the glass fiber filters, the impinger solution samples, pretest smears of the off-gas lid and line, pretest SUMA can analysis, and pretest samples of the cover blanket insulation. The samples were analyzed for Hg, lanthanides, nitrates, sulfates (impinger solutions only), and organics (soils only). These components were analyzed to provide background data for subsequent evaluations of thermal transport of inorganic and organic materials through the soils. Both lanthanide and Hg compositions were determined using inductively coupled plasma/mass spectrometry (ICP/MS); the organic compositions were determined using standard GC or GC/MS methods.

Pretest samples of the four sludge mixtures used in the test were analyzed by GC methods. The actual concentrations of four halogenated hydrocarbons (TCA, TCE, PCE, and CCl_4) were determined in the sludge mixtures because of the possibility of volatilizing some of the organics during mixing of the sludges. The target composition and the measured composition are given in Table 3.2. In these data, the analytical results are consistently higher than the expected results based on the amount of chemicals added when the sludge was prepared. The procedure for preparing the sludge has been checked, and no error has been found. Since the results are consistently high, it does not

TABLE 3.2. Pretest Sludge Composition, ppm

Sludge Series	CCl_4 (A)[a]	PCE (A)	TCA (B)	TCE (C)	Hg (A)
Series A					
Expected Conc.	11.9E3	2.32E3	0	0	16800
Analyzed Conc.	25.3E3	10.1E3	<1.6E3[b]	<1.6E3	NA
TCLP-ZHE	195	22.7	<5	<5	165
Series B					
Expected Conc.	0	0	10.6E3	0	
Analyzed Conc.	<1.6E3	<1.6E3	23.1E3	<1.6E3	
TCLP-ZHE	<12.5	<12.5	393	<12.5	
Series C					
Expected Conc.	0	0	1	11.8E3	
Analyzed Conc.	<3.1E3	<3.1E3	<3.1E3	31.0E3	
TCLP-ZHE	<12.5	<12.5	<12.5	337	

(a) Letter in parentheses indicates series.
(b) Values with less than (<) symbols are below calibration limits for the composition scale used.

appear likely the problem was due to sampling. A potential cause is the significant dilution that was required to analyze for these materials at these concentrations. Another potential cause for this variation is potential sludge inhomogeneities during mixing. As a result, the added concentrations for each of these components were used instead of the analyzed concentrations. The concentrations of lanthanides and Hg in the sludges were not determined because a simple mass balance of the material added was considered sufficient.

The ICP/MS analytical procedure involved sample preparation in accordance with PNL QA Procedure 7-40.45. The GC and GC/MS procedures involved sample preparation in accordance with EPA SW846 Method 5030, followed by analytical testing in accordance with EPA SW846 Method 8240. In addition, pretest samples of the sludge mixtures were leach tested in accordance with TCLP (for Hg) and TCLP-ZHE procedures for halogenated hydrocarbons. This was required to compare the posttest quality of the soil with the pretest quality of the sludge mixtures. The TCLP and TCLP-ZHE samples were prepared in accordance with 40 CFR 268, App. I, then either analyzed for organics (EPA SW846 Method 8240) or Hg (EPA SW846 Method 7470).

The average oxide composition of INEL soil determined from previous ISV tests is given in Table 3.3. This analysis provides a background for comparison with the ISV vitrified product and also indicates that the soil alone contains an appropriate proportion of glass formers, such as silicon and aluminum oxides, and glass modifiers, such as sodium, potassium, and calcium oxides, to form an acceptable ISV product. No amendments are required for this application.

3.4 POSTTEST SAMPLING

At the completion of the test, the electrodes were left in the melt until the melt had cooled. The NO_x analyzer and the MM5 sampling system were turned off immediately after the shut down of power. The SUMA canister continued to operate for 24 h after the test was complete. The off-gas system continued to be operated until the vitrified block was excavated.

TABLE 3.3. INEL Soil Oxide Composition

Oxide	wt%
Al_2O_3	11.85
B_2O_3	0.05
BaO	0.09
CaO	3.68
Cr_2O_3	0.02
Fe_2O_3	4.25
K_2O	2.99
MgO	1.72
MnO_2	0.10
Na_2O	1.37
NiO	0.04
SiO_2	62.60
SrO	0.02
TiO_2	0.68
ZrO_2	0.05
Total	89.50
Moisture	7.5

After shutting down the off-gas system, the off-gas samples were prepared and sent to the analytical laboratory. Samples from the inorganic sampling train included particulate filter samples and impinger solution samples; these were analyzed by ICP/MS procedures and included both nitrate and sulfate analysis. The organic sampling train included only the SUMA can samples that were analyzed by GC/MS methods. Samples of the cover blanket insulation, 25 cm^2 (4 $in.^2$), were taken and analyzed by ICP/MS. Smear samples of the off-gas lid and off-gas lid line were also taken but were not analyzed.

During excavation of the vitrified block, samples of the vitrified material and the surrounding soils in both the horizontal and vertical directions were obtained and packaged in accordance with the EG&G Sampling and Analysis Plan (SAP). The soil was removed in layers until either the thermocouples on the soil side were exposed or the extended canister layer was exposed. A modified core sampler of 3.8-cm (1.5-in.) diameter PVC pipe was used to take the surrounding soil samples. The surrounding soil samples were taken at approximately the 350°C, 150°C, 100°C, and 50°C isotherms directly beneath the melt, and at a depth of 35.6 cm (14 in.) on both the soil and canister sides of the melt (see Figure 3.5). The exact locations of these samples were based on maximum readings on horizontal Type K thermocouples; the approximate locations are shown in Figure 3.6. Samples from each position were prepared for analysis by ICP/MS, TCLP, TCLP-ZHE, and GC procedures.

Upon removing the ISV glass block from the engineering-scale container, the block was photographed and weighed, and the dimensions were measured. Glass phase samples from the block were taken in accordance with the EG&G SAP. The approximate location of the glass samples is shown in Figure 3.6. The samples were sealed, packaged, identified, and sent to the analytical laboratory for analysis (according to the EG&G SAP).

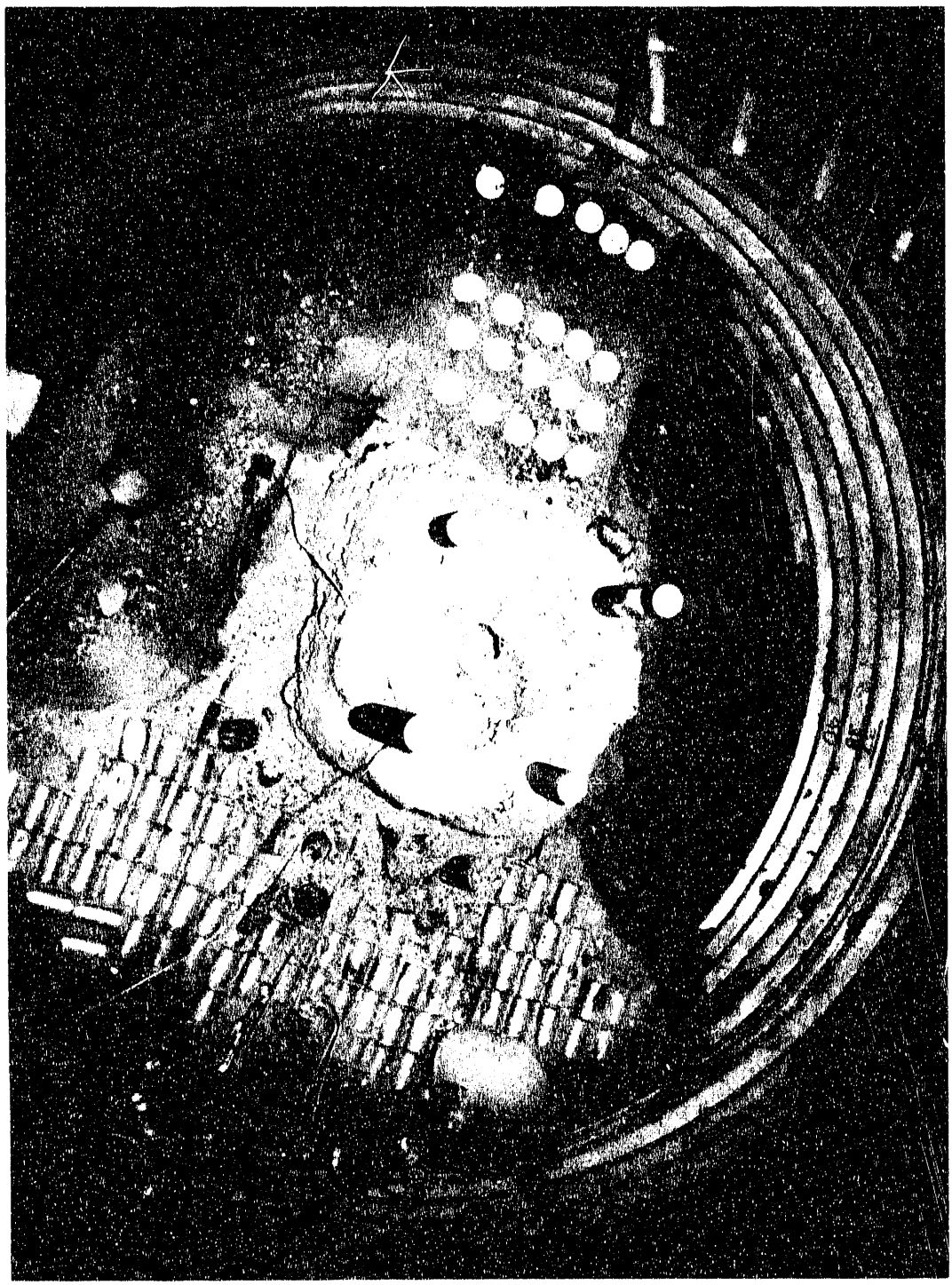

FIGURE 3.5. Soil Sampling Locations for ES-INEL-5

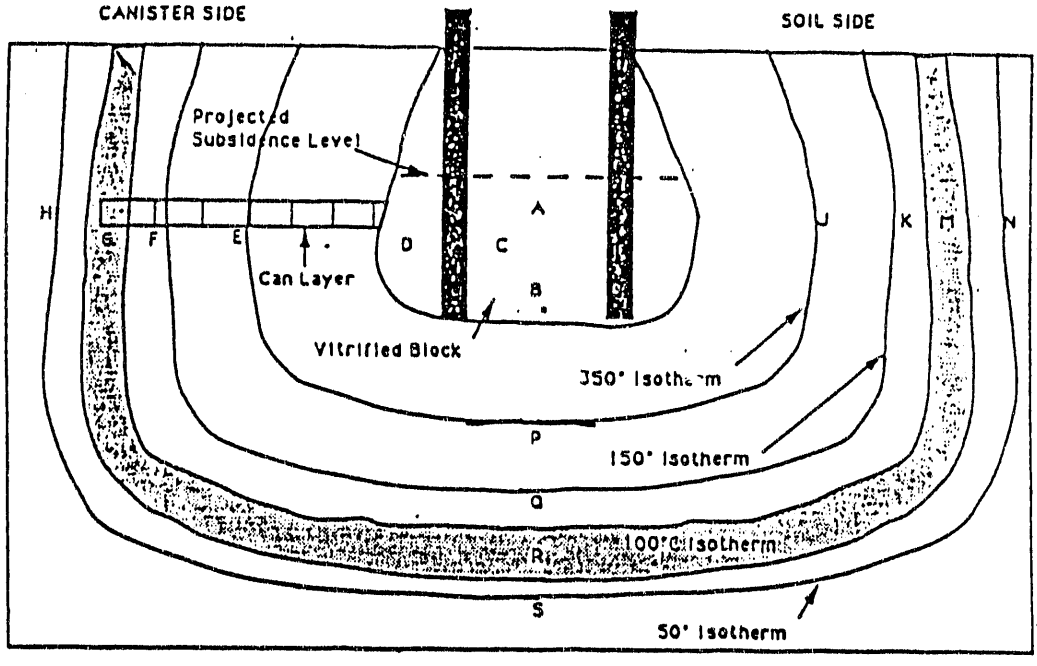

FIGURE 3.6. Posttest Sample Locations for ES-INEL-5

4.0 PROCESS RESULTS

4.1 OPERATIONAL CHRONOLOGY

ES-INEL-5 was started at 5:30 p.m. on September 18, 1990, and completed at 12:42 p.m. on September 20. Two restarts were performed. The total time power applied to the block was 25 h. The test was performed in accordance with PNL Test Plan ES-INEL-5, Rev. 0 (May 1990), INEL Sampling and Analysis Plan EGG-WM-9091 (June 1990), and PNL Technical Sampling Procedure for Engineering-Scale ISV Tests (PNL-ISV-1, December 1989).

4.1.1 Test Performance

The following is a chronology of the events of ES-INEL-5.

September 18, 1990

17:30. ES-INEL-5 was started. A typical starter path, 2.5 cm x 2.5 cm (1 in. x 1 in.), was used and functioned normally.

21:16. Power to the melt was shut off due to a broken electrode. The attempt at a restart failed and the melt was allowed to cool down to lay a new starter path.

September 19, 1990

08:12. The test was restarted.

12:08. MM5 off-gas sampling was started.

12:38. Organic vapor sampling (critical orifice SUMA can) was started.

14:15. Powered operation was suspended due to positive pressure venting into the workplace atmosphere. These pressurizations were caused by rapid (less than 0.5 s) releases of gases from the rupturing of the test cans.

14:20. A sample of the off gas was taken during venting.

16:30. The workplace atmosphere was monitored and found to be safe.

17:00. The engineering-scale container was resealed and a restart attempted. This restart failed, so power was shut off and a new starter path laid.

21:30. The test was restarted.

September 20, 1990

3:30. Test can ruptures began again. Workplace air monitoring confirmed a safe environment. Power was reduced. Can ruptures continued for approximately the next 12 h.

12:42. The test was concluded 1 h after the thermocouple located at 53 cm (21 in.) had reached 1200°C.

4.1.2 Standard Performance Data

During ISV processing the block reached a depth of 58 cm (23 in.) and a width of 61 cm (24 in.), with full surface subsidence to a depth of 28 cm (11 in.). The vitrified block weighed approximately 224 kg (494 lb). A photograph of the block is shown in Figure 4.1.

Performance data for ES-INEL-5 are shown in Table 4.1. For comparison purposes, the performance data for ES-INEL-4 (Shade et al. 1991) are also shown. The energy-to-mass ratio of the resultant block was 1.4 kWh/kg soil as compared to 1.3 kWh/kg of soil in ES-INEL-3 and ES-INEL-4. The difference is likely due to remelting the previously melted soil in the test restarts.

Electrical data for ES-INEL-5 are illustrated in Figure 4.2. The test ran for 25 h, in periods of 3.8, 6.0, and 15.2 h over a 43.2-h period. Powered operation was suspended for 14.7 h due to the broken electrode and 7.2 h due to the positive pressure venting.

Electrode oxidation was observed at the glass interface inside the subsidence area. Two-in. diameter uncoated graphite electrodes were used. At the areas of greatest oxidation, the diameters were 1 5/8 in. for the NE electrode, 1 5/8 in. for the NW electrode, 1 1/8 in. for the SW electrode, and 1 3/4 in. for the NE electrode.

4.2 TEST OBJECTIVES - RESULTS/INTERPRETATIONS

Seven objectives were identified for ES-INEL-5. The test results as they relate to these objectives are discussed below.

How do the pressurized releases from sealed containers affect the off-gas composition, and how do the releases affect the pressure and temperature of the hood plenum?

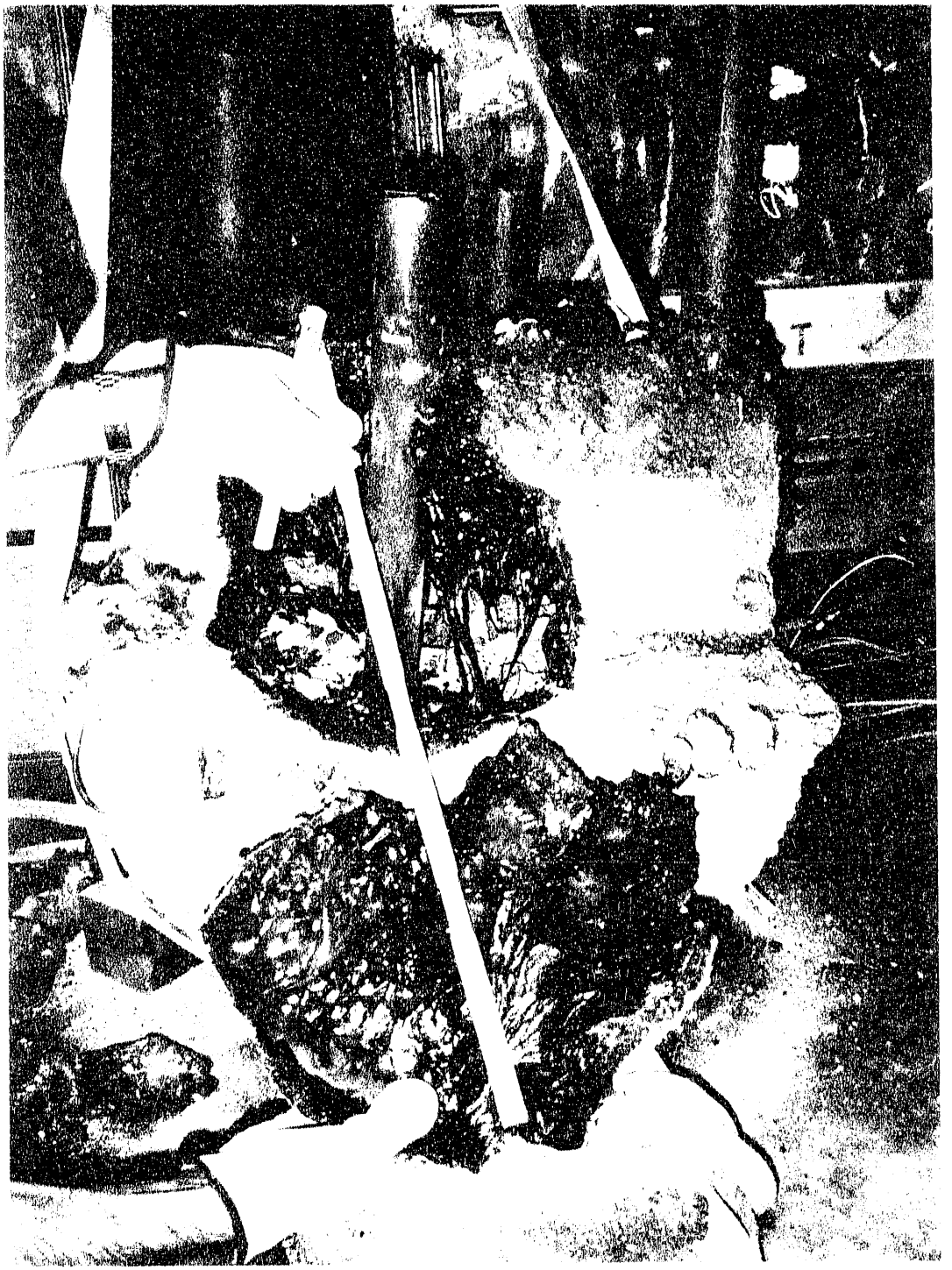

FIGURE 4.1. Vitrified Block

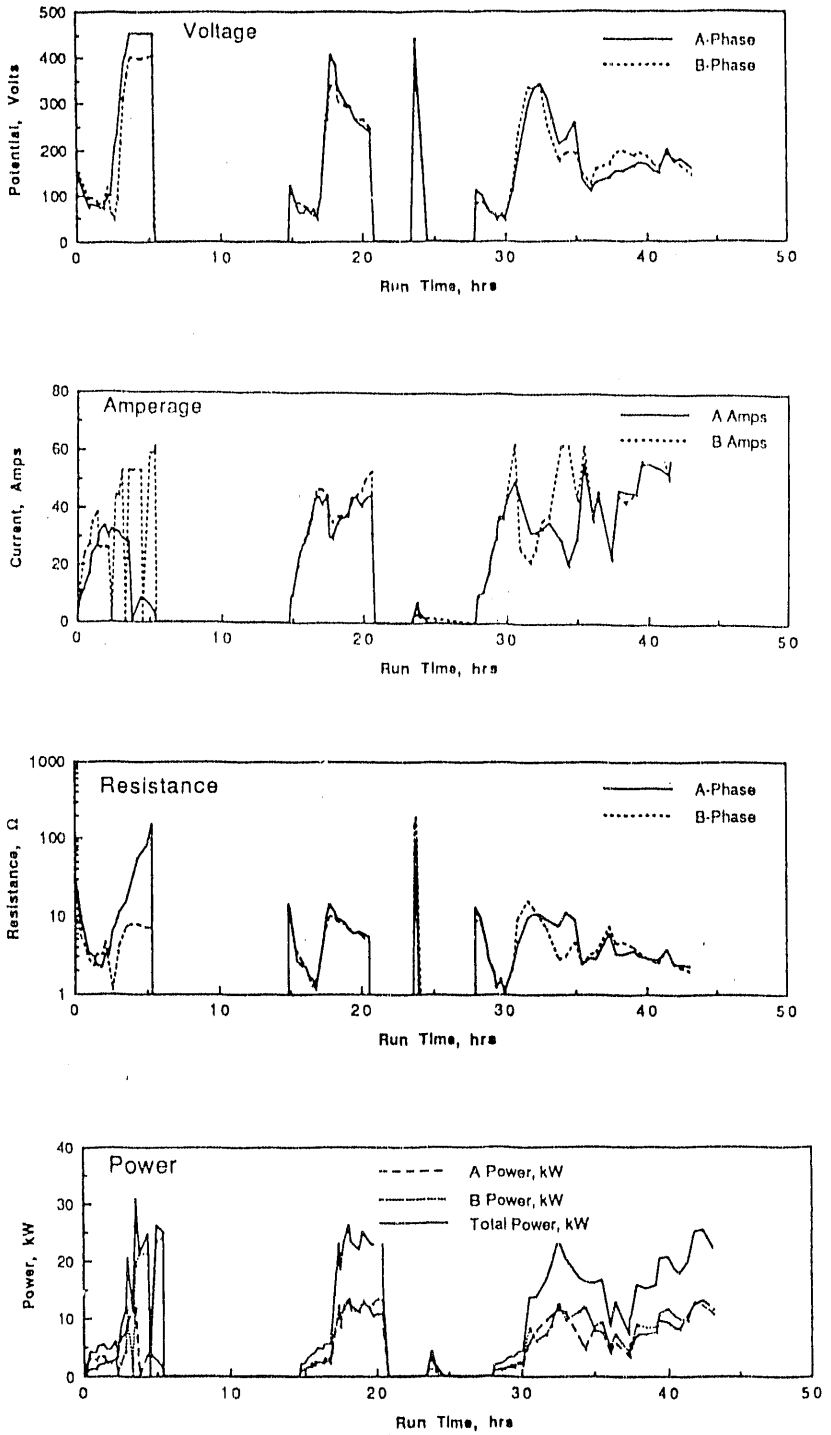

FIGURE 4.2. Electrical Data for ES-INEL-5

TABLE 4.1. Performance Comparison of Engineering-Scale Tests

Parameter	ES-INEL-4[a]	ES-INEL-5
Total run time, h	41.1	25
Total energy, kWh	585	317
Melt depth, m (in.)	0.79 (31)	0.58 (23)
Melt width, m (in.)	0.81 (32)	0.61 (24)
Surface subsidence, m (in.)	0.38 (15)	0.28 (11)
Vitrified glass weight, kg	407	224
Soil vitrified (est.), kg	456	251
Energy-to-mass ratio, kWh/kg	1.3	1.4

(a) Shade et al. 1991.

Hood and can pressure data were taken once every 0.5 s. For two instrumented cans, Can A and Can C, the release of the pressure from the cans corresponded to a pressurization of the hood (Figures 4.3 and 4.4). None of the other instrumented cans showed a relationship between release of canister pressure and hood pressure. Only a few of the canisters (Cans B, D, and I) showed any significant build-up of pressure at all. The pressure instrumentation in the other canisters may have failed causing either the canisters to leak or the pressure sensors to read incorrectly. Cans A and C showed a very rapid release of pressure (less than 0.5-s duration), which indicates a rupture of the canister. For Cans B, D, and I, the pressure releases were much slower. This indicates that for this scale of test with this quantity of gas released in order to pressurize the hood, the release of gases from the canister must be very rapid.

Hood pressure data showed 51 separate incidents of hood pressurization. (Some incidents had more than one positive pressure point. Positive pressures that occurred 0.5 s apart--the data sampling frequency--were assumed to be the same incident.) Therefore, approximately 25% of the total 200 test canisters ruptured with sufficient force to pressurize the hood. This is approximately twice the rate of the instrumented cans (2 out of 15 or about 13%), which is another indication that the pressure instrumentation on several of the canisters may have failed.

Posttest observations were made of the 200 test canisters (see Figure 4.5). The 24 Series A cans were all incorporated into the melt. All

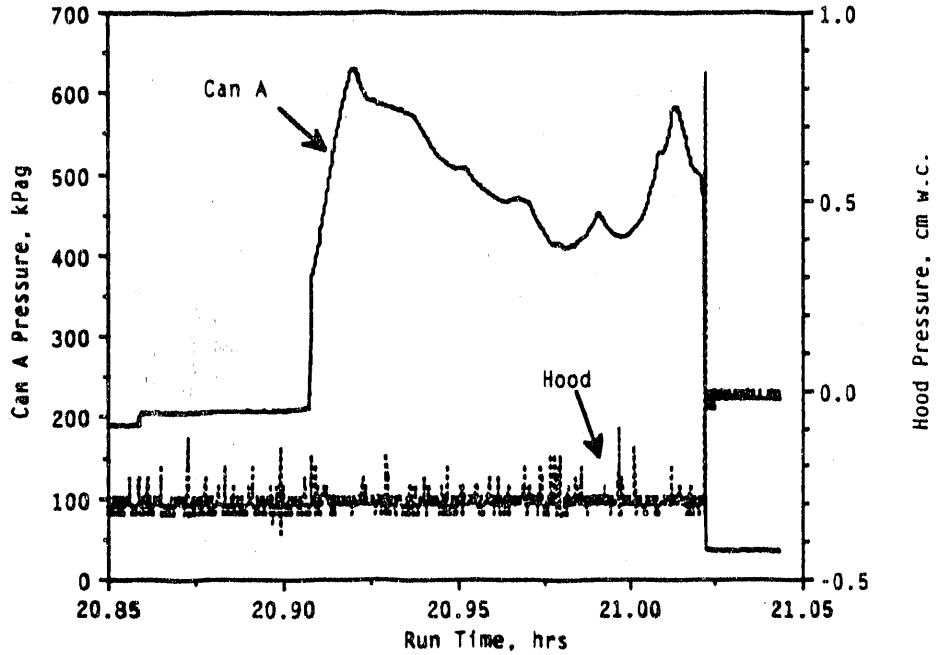

FIGURE 4.3. Can A Pressure and Hood Pressure

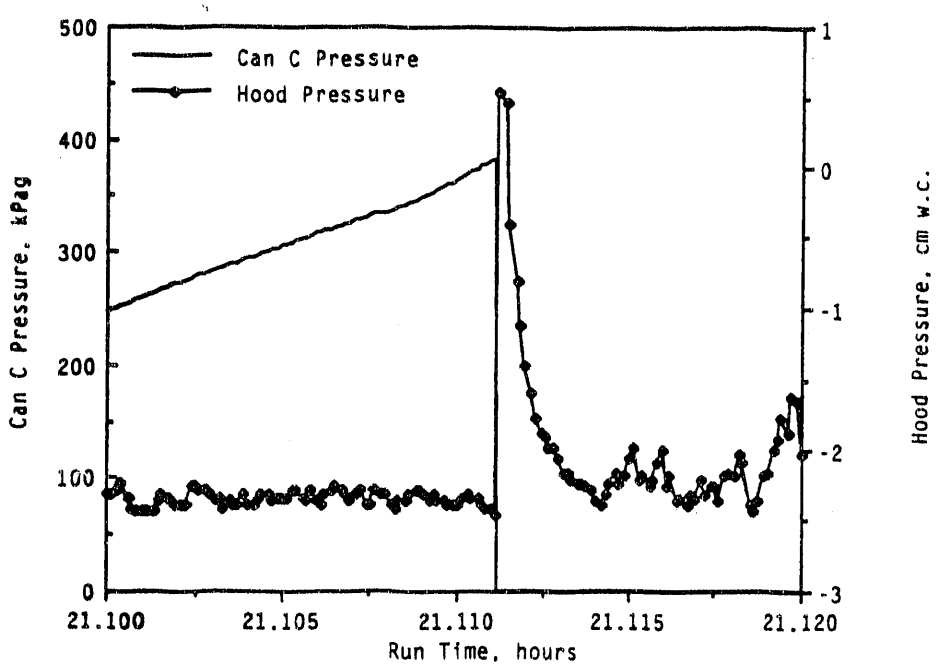

FIGURE 4.4. Can C Pressure and Hood Pressure

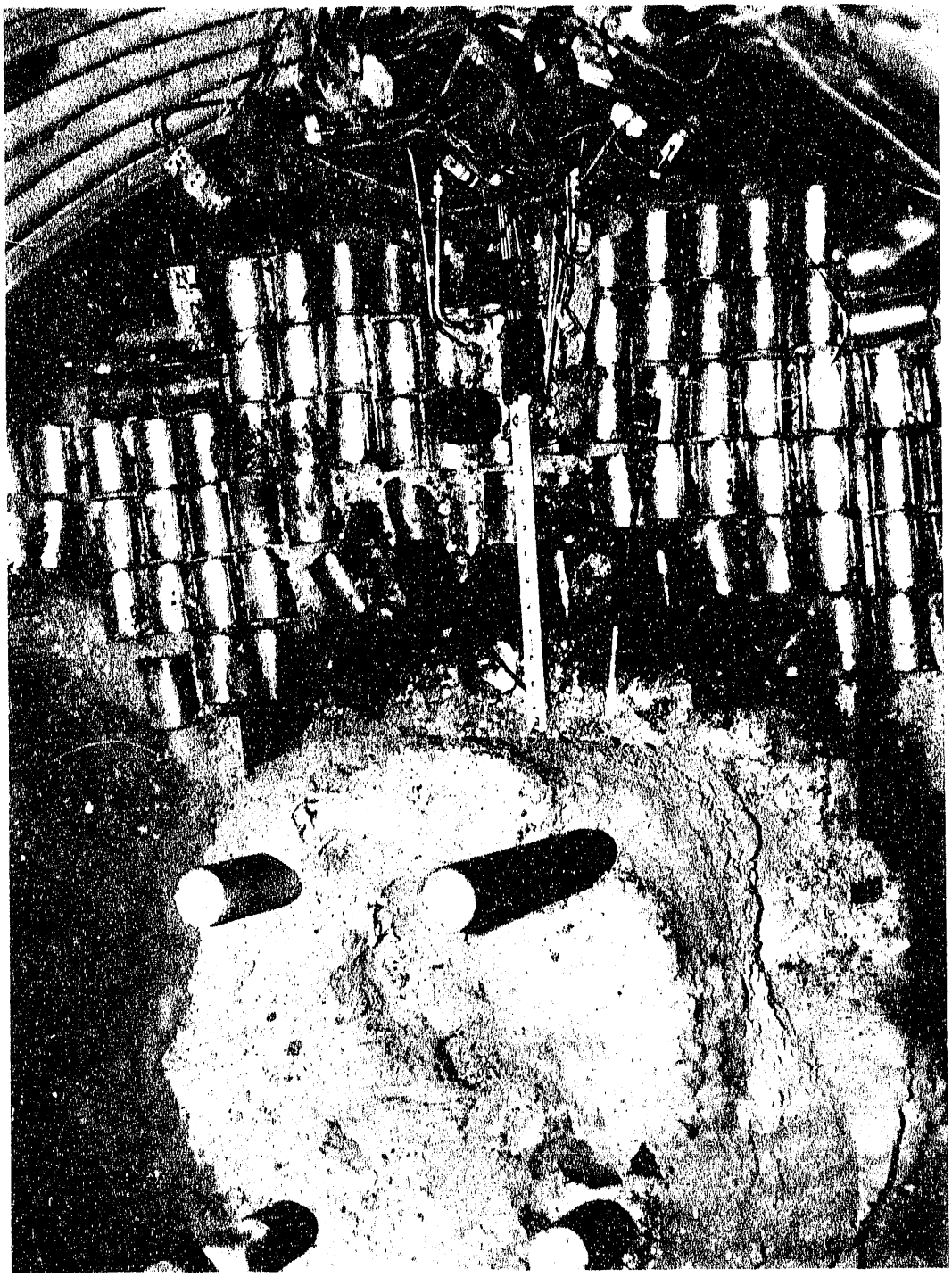

FIGURE 4.5. Photo of Posttest Canisters

except one (out of 64) of the Series B cans were partially incorporated into the melt. The one not incorporated was blown. Of the Series C cans (48 total), 25 were unpressurized, 10 were pressurized, 8 were ruptured, and 5 had pinhole leaks. Thus 87 cans were totally or partially incorporated into the melt and 9 additional cans were ruptured, giving a total of 96 cans which could potentially have pressurized the hood. Fifty one pressurizations, or 53% of this total, actually occurred.

To determine if this percentage was representative of a full-scale application, the nature of the release must be analyzed. The first determination must be the amount of gas released (and at what temperature) to cause the pressurization. Because of the complex nature of the sludge mixture in the canisters, it is difficult to establish directly how much gas may have been released. However, an analysis can be made of the response of the hood pressure to the rupture of Can C (Figure 4.6) to determine this amount.

By mass balance, the accumulated gas released to the hood is equal to the off-gas flow out of the hood minus the air flow into the hood integrated over the time of the event.

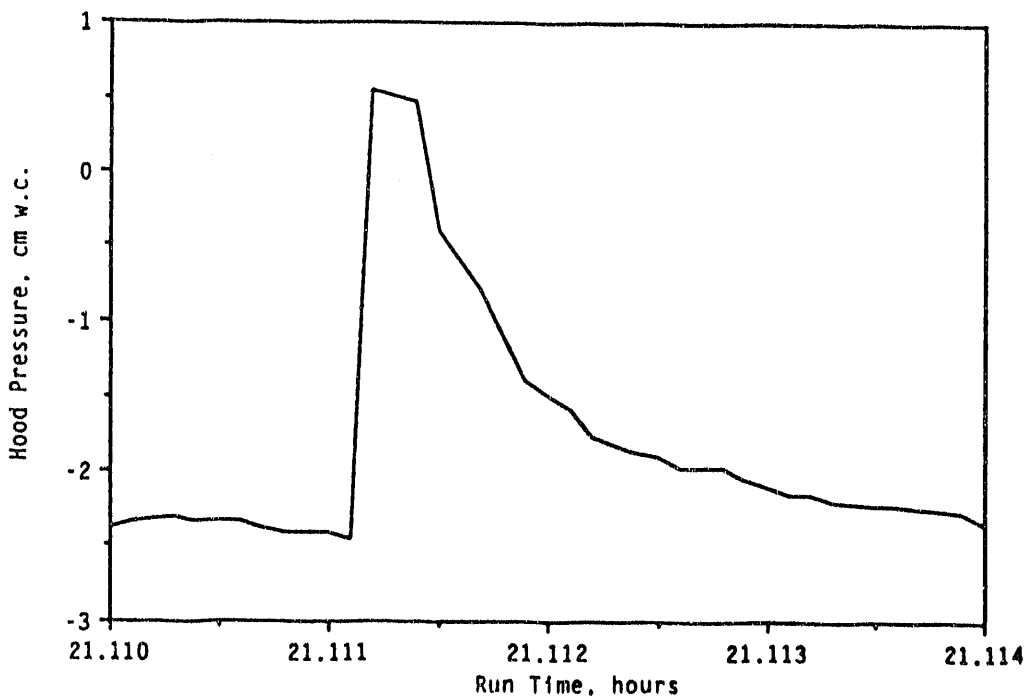

FIGURE 4.6. Hood Pressure Response from Can C Rupture

This is given by the equation:

$$\int dN_{hood} = \int (F_{off\ gas} - F_{air\ in}) \cdot dt \qquad (4.1)$$

where N_{hood} = the moles in the hood in gmoles
$F_{off\ gas}$ = the flow rate through the off-gas system in gmoles/min
$F_{air\ in}$ = the flow rate of air into the hood in gmoles/min
t = time in min.

The air flow into the hood is a function of the pressure in the hood. If we assume that this relationship approximates that of flow across an orifice, then the air flow is proportional to the square root of the pressure drop between the hood pressure and atmosphere (Darcy's formula).

This relationship is supported by comparing the pressure in the hood at two different off-gas flow settings. At the start of the test, the pressure in the hood was approximately -0.30 cm w.c. (-0.12 in. H_2O) at an off-gas flow of 0.637 m^3/min (22.5 scfm). At the time Can C ruptured, the hood pressure was approximately -2.41 cm w.c. (-0.95 in. H_2O) at an off-gas flow of 1.84 m^3/min (65 scfm). The square root of the ratio of the pressure drops is 2.81 compared to the ratio of the flows, which is 2.89.

In the initial case, we assumed that the flow of air into the hood was equal to the off-gas rate (1.84 m^3/min) and the pressure drop equal to that of the hood pressure (2.41 cm w.c.). From this, flow of air into the hood can be calculated for any pressure in the hood using:

$$F_{air\ in} = 76.3\ gmoles/\text{min} \cdot \sqrt{P_{hood}/2.41} \qquad (4.2)$$

where $F_{air\ in}$ = the flow of air in gmoles/min
P_{hood} = the pressure of the hood in cm w.c. vacuum
76.3 gmoles/min = 1.84 m^3/min
2.41 = the initial hood vacuum in cm w.c.

Initially, flow is actually out of the hood (since the hood pressure is positive). To calculate the flow in this case, the same square root relationship

is assumed; however, the flow is corrected for temperature. Equation (4.2) is multiplied by the square root of 294/509, where 294K is the temperature at standard conditions and 509K is the temperature of the hood. (The gas flow is proportional to the square root of density. Using the ideal gas law, density is inversely proportional to temperature. The gas composition in the hood is assumed to be close to that of air, and the pressure is close to atmospheric, so the correction for pressure and molecular weight was neglected.)

The net flow out of the hood is the off-gas flow minus the flow of air into the hood. This is calculated assuming the off-gas flow remains constant. Since the downstream vacuum in the off-gas system is high (approximately 203 cm w.c.) compared to the changes in hood pressure, it can be assumed that the off-gas flow rate will not change significantly throughout the event. The air flow into the hood and the net flow out of the hood are plotted in Figure 4.7.

The relationship of net flow out of the hood with time follows an inverse square root function (plotted in Figure 4.8). From this relationship,

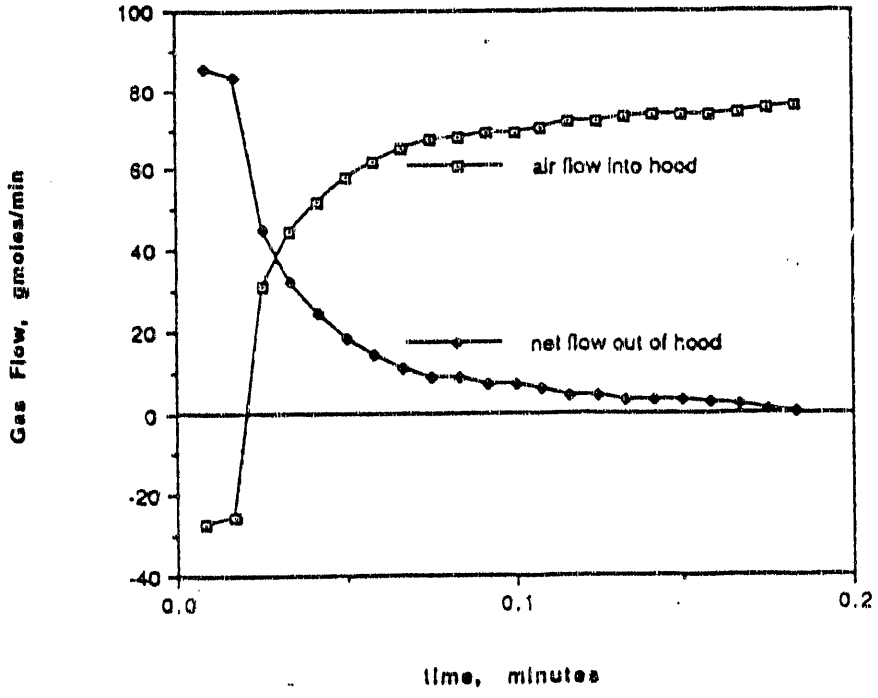

FIGURE 4.7. Calculated Gas Flows After Can C Rupture

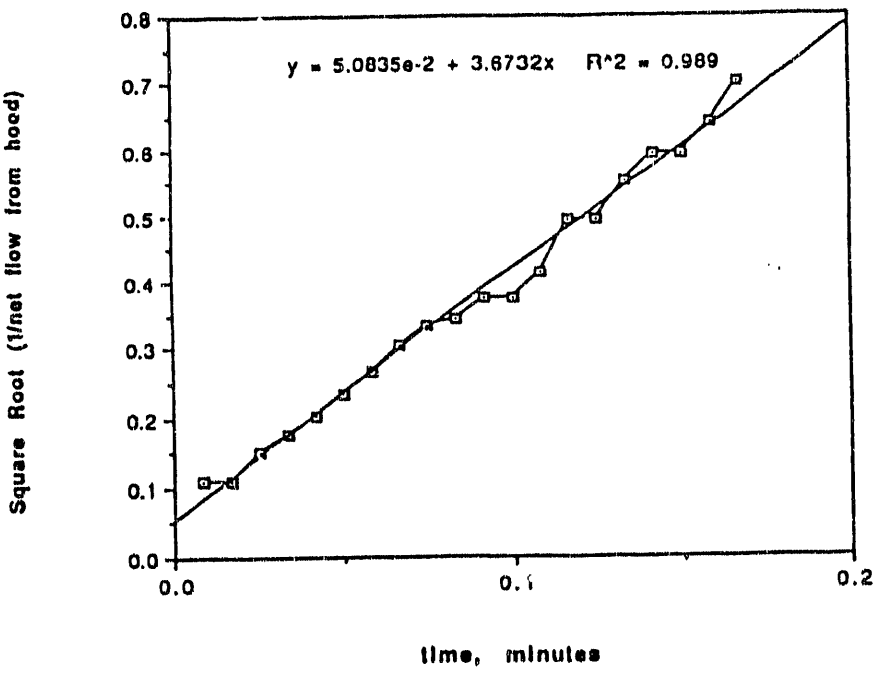

FIGURE 4.8. Gas Flow Relationship with Time

the initial net flow of gas from the hood can be determined directly, and the total gas released can be calculated by integration. (The calculated total gas released is obtained from this integration.)

This calculation is sensitive to the assumed time of initial release, which can differ by up to 0.5 s. The range of potential values is given below.

At time = 0 (last low-pressure reading)

Initial net flow out of hood = 311 gmoles/min (265 scfm)

Total gas released = 5.4 gmoles

Initial hood pressure = 69.1 cm w.c. (27.2 in H_2O)

At time = 0.5 s (highest recorded hood pressure)

Initial net flow out of hood = 151 gmoles/min (129 scfm)

Total gas released = 3.3 gmoles

Initial hood pressure = 3.96 cm w.c. (1.56 in H_2O)

As can be seen, the calculated gmoles released differs by about 2 gmoles or almost 40%, which is significant for evaluating the nature of the gas release. Fortunately, there is an independent method to determine which value is more correct.

The initial hood pressure given above is calculated by working backwards from the square root relationship discussed earlier. Using this initial hood pressure and the calculated moles of gas released, the total system volume (i.e., the volume of the ISV engineering-scale system) can be estimated and compared to the actual volume of the system. This comparison can then be used to determine which value (time = 0 or time = 0.5) is most correct. The calculated system volume assuming two different gas temperatures is given in Table 4.2. As can be seen in Table 4.2, the actual gas release is closer to the time = 0 value of 5.4 gmoles.

This is true even if a higher gas temperature is assumed. The actual temperature of the releasing gases is unknown; however, the hood plenum temperature does not change significantly (approximately 1.2°C, see Figure 4.9) during the Can C rupture. A heat balance was not attempted since it is believed that the pressurization dispersed gas throughout the test system, including the voids in the soil. Therefore, much of the heat may have been dissipated to the soil particles.

To further understand the nature of the release, a comparison can be made between the estimated release of 5.4 gmoles and the contents of the can. Several scenarios can be proposed. One is that the release was simply due to the release of the pressurized gas in the canister. Using the ideal gas law

TABLE 4.2. Calculated System Volumes Versus Actual System Volumes

Assumed Gas Temperature	Calculated System Volume, m^3	
	Time = 0	Time = 0.5
264°C	3.4	23.8
100°C	2.4	16.6
Actual hood plenum volume = 1.7		
Total system volume assuming 50% void space in soil = 4.2		

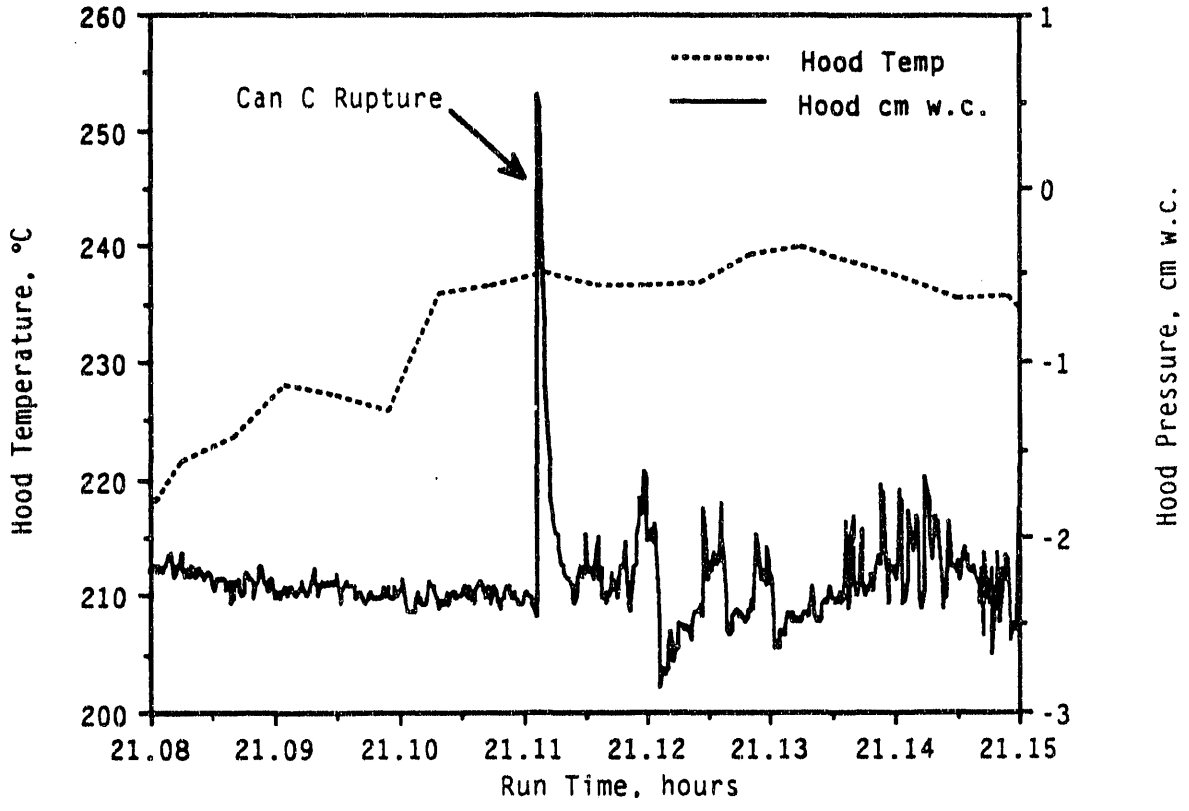

FIGURE 4.9. Hood Temperature and Pressure During Can C Rupture

and assuming that the total volume of the can contained gas at the pressure and temperature of the can before the release, the calculated gmoles is only 0.02 gmoles. Therefore, it is improbable that the release was only due to pressurized gas.

Another scenario is that the volatile components in the can vaporized during the canister rupture and contributed to the gas release. The major volatile components were H_2O (2.09 gmoles) and CCl_4 (0.16 gmoles). The gmoles of the other volatile components were insignificant. As can be seen, these also do not account for the gas release.

The major remaining scenario is that components in the sludge reacted to produce additional gas. The likely candidates are the nitrates and the organics. To assess this possibility, the fate of the nitrates can be determined.

Figures 4.10 and 4.11 show the NO_x releases for ES-INEL-5. The peaks are associated with the rupture of individual cans. Specific peaks can be associated with the rupture of two instrumented cans, Can A and Can C (see

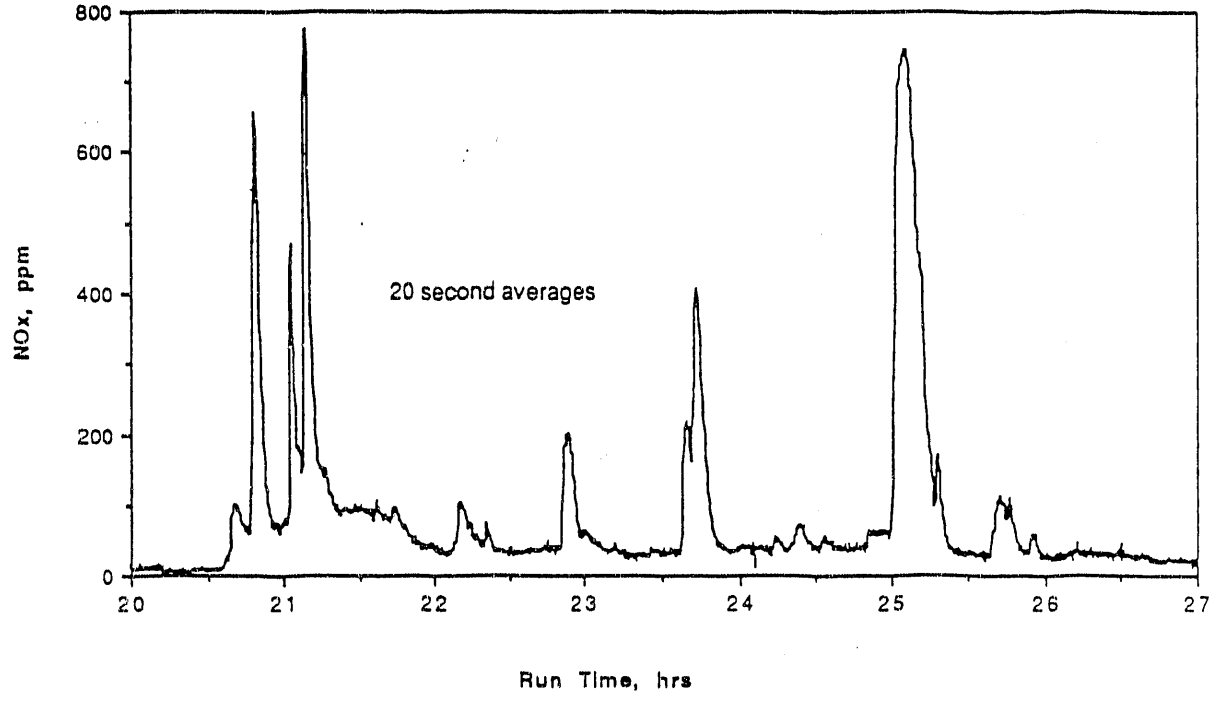

FIGURE 4.10. NO_x Concentration in the Off Gas (20-s averages) Early in Test

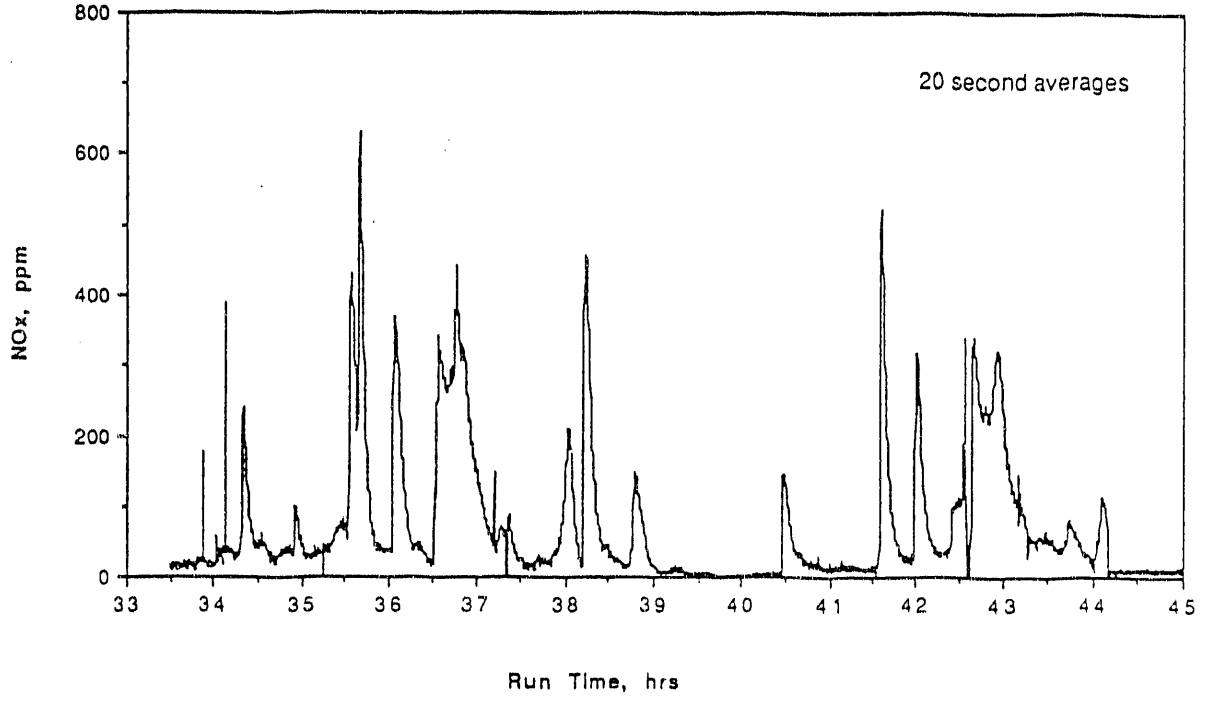

FIGURE 4.11. NO_x Concentration in the Off Gas (20-s averages) Late in Test

Figure 4.12). In the case of Can C, most of the NO_x was captured by the off-gas system, since the hood pressure associated with this canister burst was only momentarily positive. The NO_x curve for Can C is given in Figure 4.13. Knowing the off-gas rate, this curve can be integrated to determine the total NO_x released. This gives 0.15 gmoles NO_x. The theoretical amount of NO_x based on the nitrates in the canister was 0.638 gmoles. Thus, approximately 76% of the theoretical maximum NO_x was destroyed.

If it is assumed the destroyed nitrates reacted with the organics, several reaction gas-release scenarios can be proposed. The scenarios are described below, and the calculated gmoles are given in Table 4.3.

1. Carbon in the UnoCal Soluble 10 Oil and Texaco Regal Oil reacts with oxygen from the nitrates to produce carbon monoxide (CO). The remaining hydrogen in the oil releases as gas. Water releases as vapor. The CCl_4 releases as vapor.

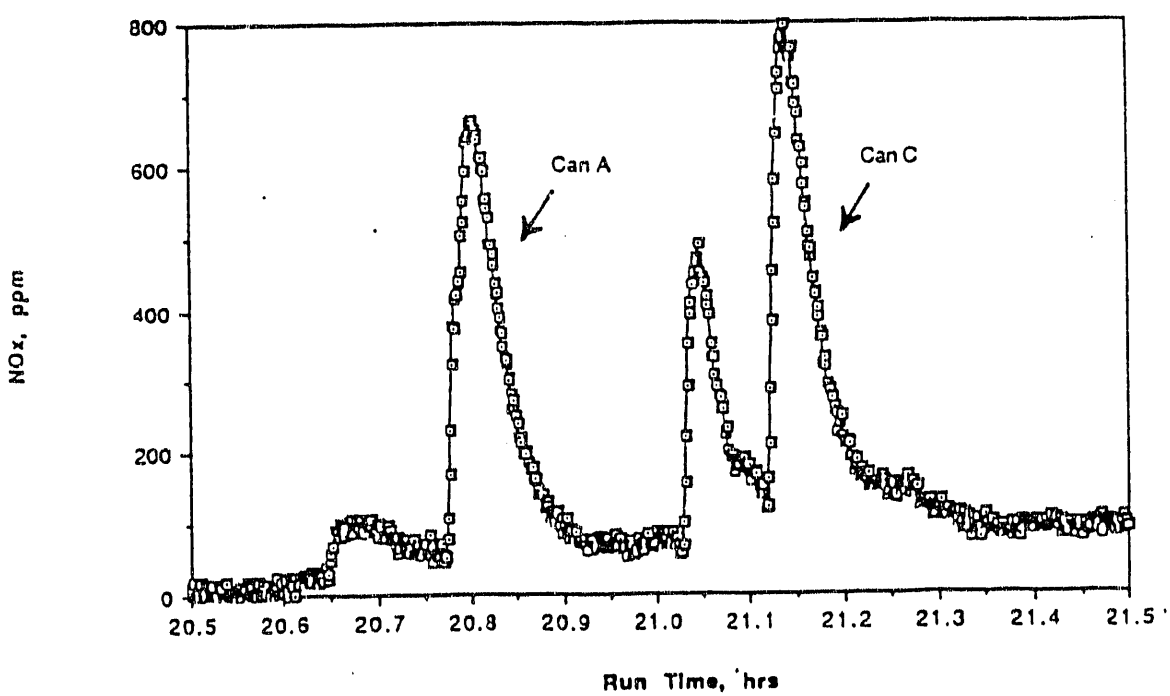

FIGURE 4.12. NO_x Concentration in Off Gas During Rupture of Cans A and C

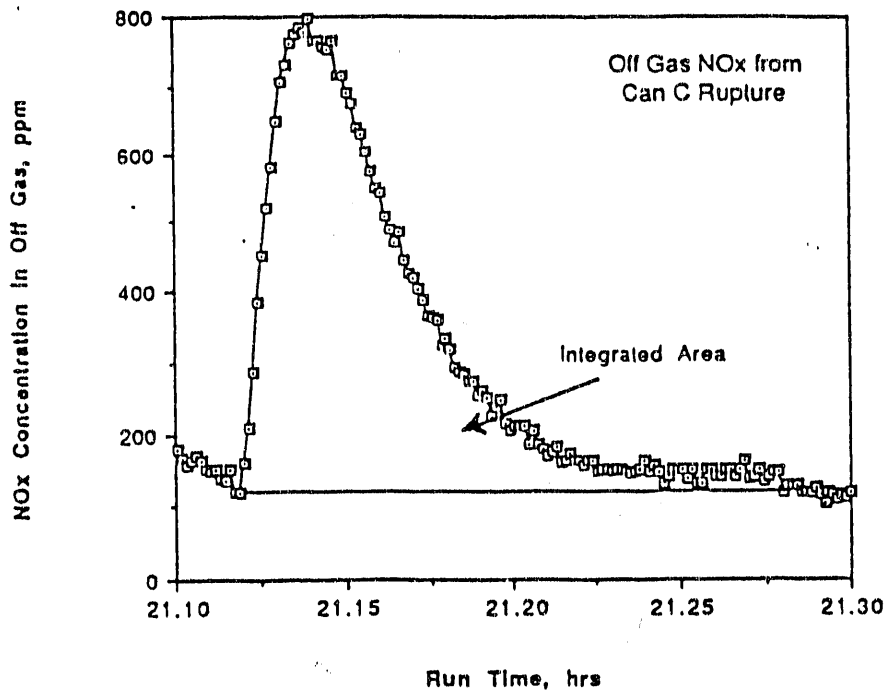

FIGURE 4.13. NO_x Integrated Area for Can C Rupture

2. Same as scenario 1, except it is assumed that the water and CCl_4 have leaked from the can prior to rupture.

3. Same as scenario 1, except that the CO and hydrogen combust with oxygen to form carbon dioxide (CO_2) and water.

4. Same as scenario 1, except that the CCl_4 hydrolyzes to form hydrochloric acid (HCl) and CO_2.

Certain assumptions were kept constant in all cases. These were:

- The gas release from the nitrates was assumed to consist of 0.15 gmoles NO_x (as NO_2) with the remaining nitrate converted to nitrogen and oxygen. This is based on the calculated NO_x release from the NO_x analyzer data.

- No release information is known for the sulfates. For the purposes of this analysis, they are assumed to convert 50% to SO_x and the remainder to sulfur and oxygen. This assumption has only a small effect on the overall balance.

TABLE 4.3. Estimated Gas Release from Can C

Scenario	Gas Released from Canister, gmole 1	2	3	4
Water	2.09	--	3.57	1.77
CO	1.67	1.67	--	1.67
CO_2	--	--	1.67	0.16
NO_x	0.15	0.15	0.15	0.15
Nitrogen	0.2	0.2	0.2	0.2
Hydrogen	1.48	1.48	--	1.48
HCl	--	--	--	0.65
CCl_4	0.16	--	0.16	--
Combustion Oxygen	--	--	(1.51)	--
Total	5.83	3.58	4.32	6.16

- The hydrogen content of the UnoCal Soluble 10 Oil and the Texaco Regal Oil is assumed to follow the equation (Perry and Chilton 1973):

$$H = 26 - 15s \qquad (4.4)$$

where s = specific gravity = 0.8762. This gives a hydrogen content of 12.9 wt%. The remainder (87.1 wt%) is assumed to be carbon.

- The contribution to the gas release of the other components in the can is assumed to be negligible.

As can be seen from these data, the estimated gas release based on a reaction of the nitrates and hydrocarbon matches well with the calculated gas released from this can. Therefore, a reaction between the organics and nitrates was likely.

It was this reaction and rapid gas release associated with it that pressurized the hood. In addition, this rapid release may have affected the concentration of NO_x in the off gas. The peak concentrations approach 800 ppm [the IDLH for NO_2 is 50 ppm (NIOSH 1990)] and appear to be associated with the rupturing of the canisters. The NO_x destruction efficiency for Can C is significantly less than has been shown in previous ISV experiments in

contaminated soil [76% versus 99.6% (Buelt et al. 1987)]. The rapid gas release created by a reaction of nitrates and organics may have been sufficient to entrain unconverted NO_x into the off gas before it was converted by the temperature of the melt.

To determine the likelihood of this reaction occurring in a large-scale application at the INEL SDA, the sludge in this test and the actual sludge in the SDA must be compared. In the SDA, the nitrates are packaged separately from the organics. In this test, the sludge was a combination of all the different SDA sludges. Therefore, the potential for the reaction to occur in the SDA is significantly less. In addition, the next section describes the pressures and temperatures in and above the canisters when they ruptured. These data indicate that the sealed nature of the canisters contributed to the likelihood of the reaction occurring. However, it still may be prudent to evaluate the impact of having nonsealed containers containing organics and nitrates in close proximity to each other.

What are the burst pressures of the carbon steel containers, and how do they relate to the temperatures inside the can and the temperature of the advancing melt front at the time of release?

Pressures and temperatures inside 15 instrumented cans (Cans A through O) were recorded by the data acquisition system. The pressures were recorded every 0.5 seconds and the temperatures every 15 s (Type K thermocouples). The melt front temperature was measured by Type C thermocouples located just above (~0.5 cm) Cans A, B, and C. These thermocouples were recorded every 5 s.

Data for Cans A, B, and C are plotted in Figures 4.14 through 4.19. (Note: Due to an improperly sized signal conditioner, the temperature plots show occasional random spikes up and down.) According to these data, Cans A and C ruptured, releasing their pressure instantly (within 0.5 s). These releases pressurized the hood. Can B pressure released more slowly and did not affect the hood pressure. Can B, however, actually reached an internal pressure as high as Cans A and B. In addition, Can D, shown in Figure 4.20, also did not rupture, and it reached a higher internal pressure than either Can A or Can C. Therefore, it is not likely internal pressure alone caused the ruptures.

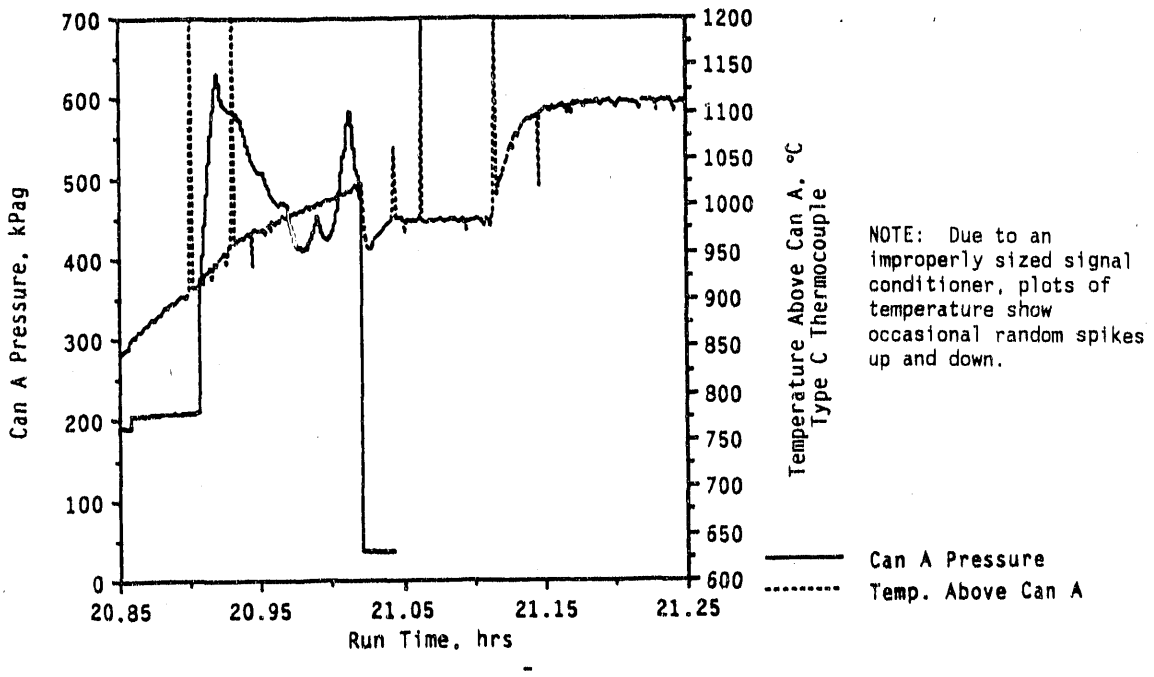

FIGURE 4.14. Can A Pressure and Melt Front Temperature Data

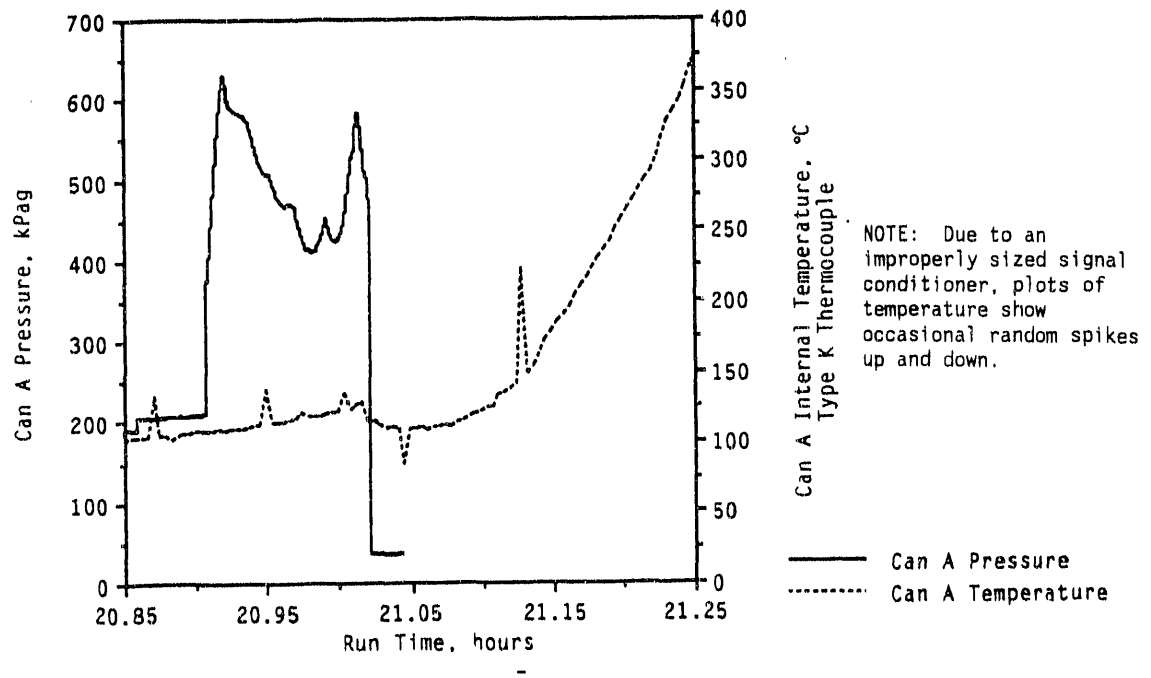

FIGURE 4.15. Can A Pressure and Internal Temperature Data

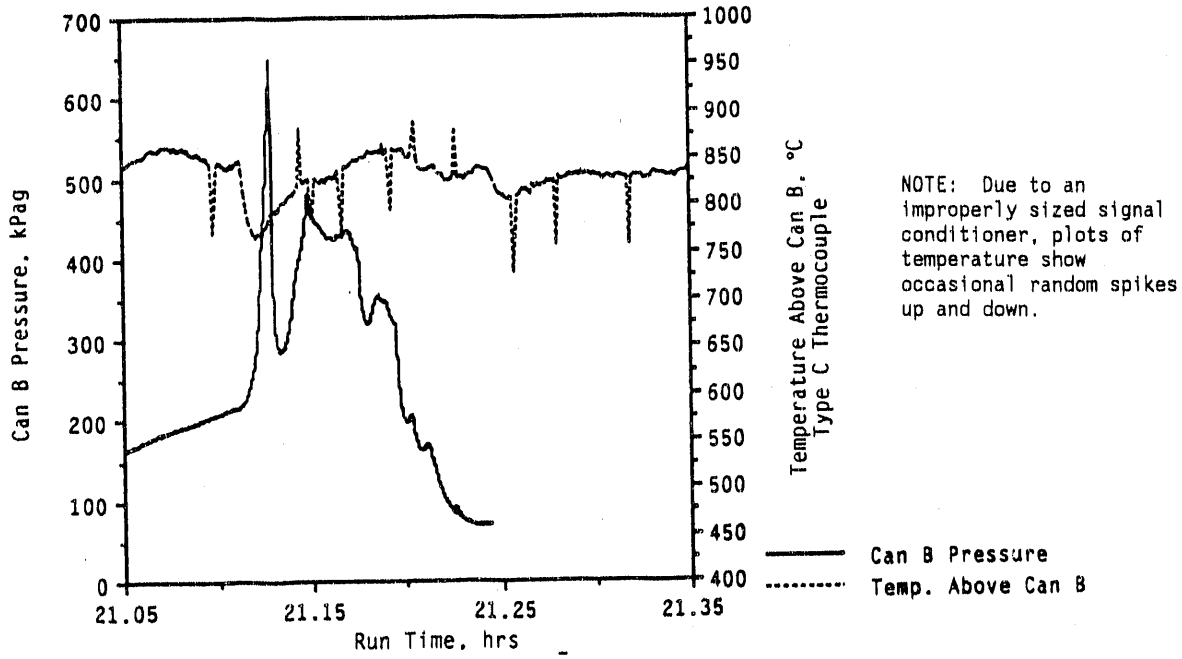

FIGURE 4.16. Can B Pressure and Melt Front Temperature Data

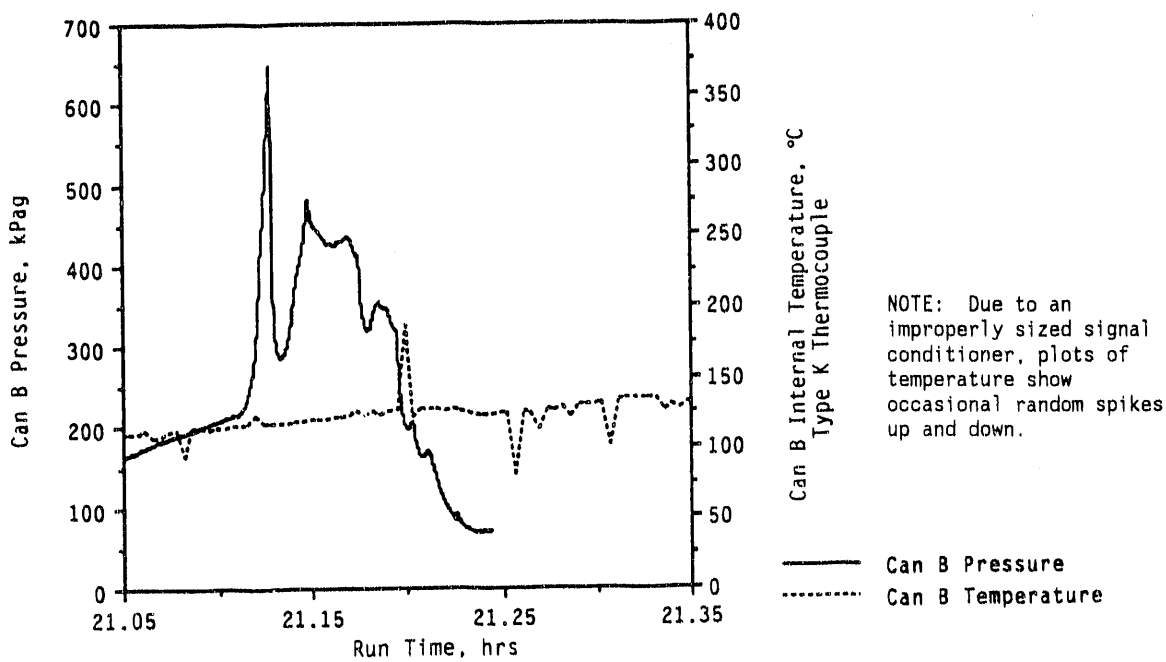

FIGURE 4.17. Can B Pressure and Internal Temperature Data

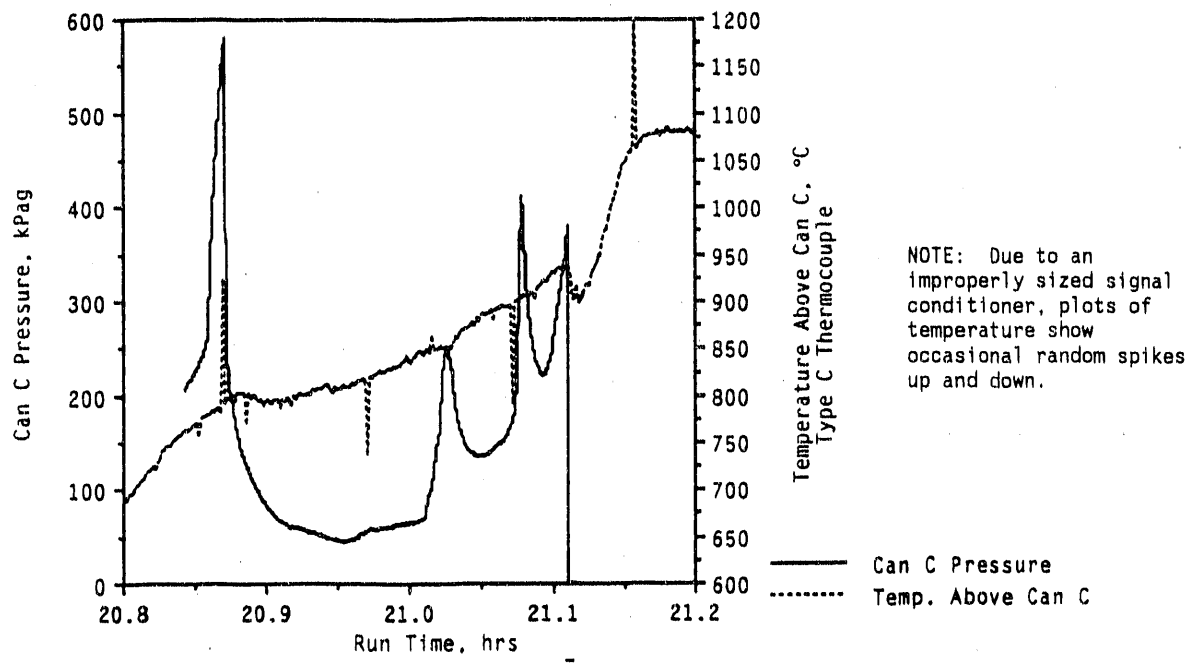

FIGURE 4.18. Can C Pressure and Melt Front Temperature Data

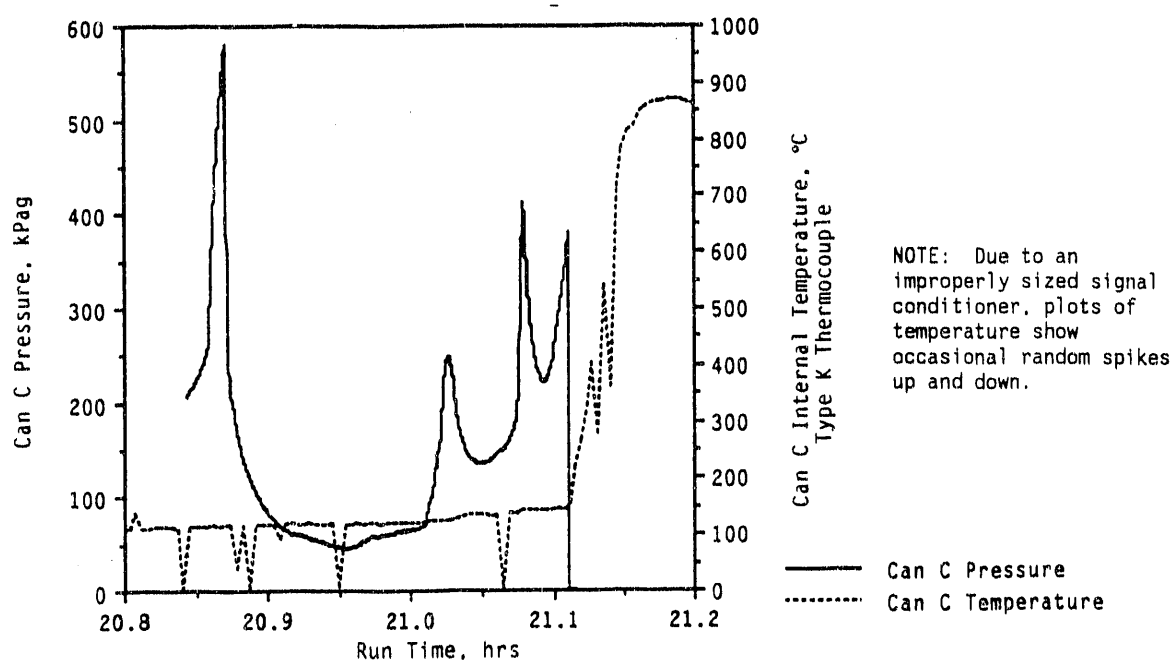

FIGURE 4.19. Can C Pressure and Internal Temperature Data

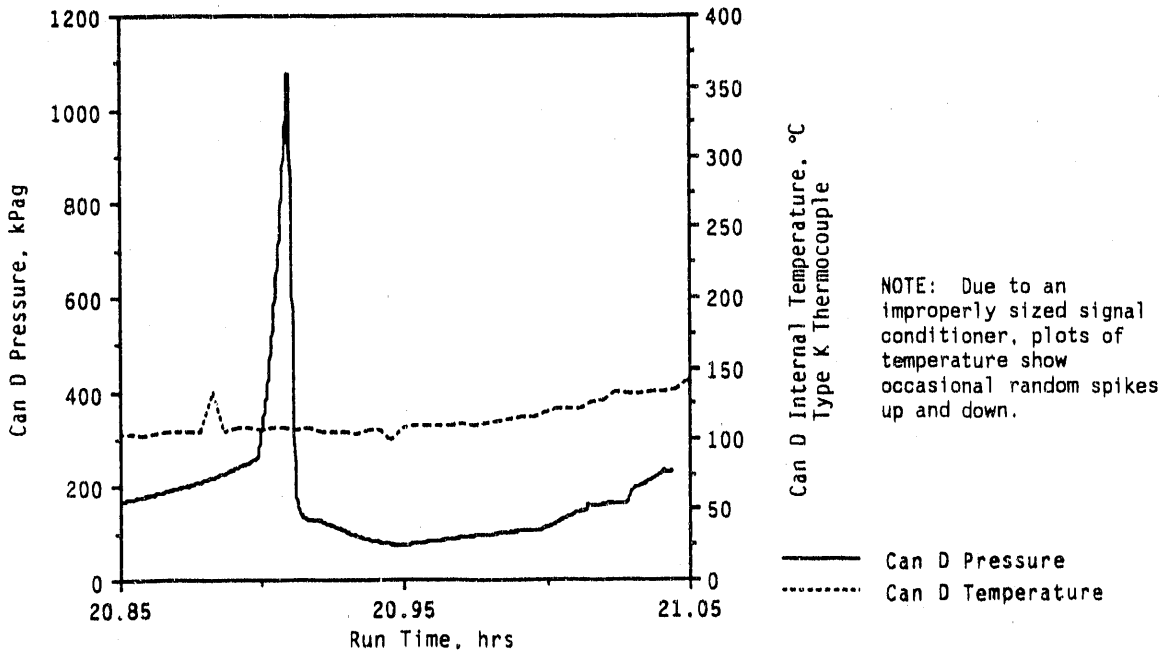

FIGURE 4.20. Can D Pressure and Internal Temperature Data

The plot of the temperature of the advancing melt front (Type C Thermocouple data) is given in Figure 4.21. As can be seen from this plot, initially the temperature above Can B was lower than for Cans A and C. Only after Can B had fully depressurized did this temperature increase to the temperatures seen for Cans A and C. Cans A and C, on the other hand, saw these higher temperatures when they were still at high pressure. Hence, it is likely that a combination of high pressure in the cans and a high melt front approach temperature was necessary to burst the canisters and pressurize the hood.

The Can B melt front temperature increased rapidly after the rupture of Can A. This may have been caused by a "stirring" of the melt due to the gases from the rupture of Can A passing through the melt. It could also be due to gases from Can A removing some of the "insulating" soil from around Can B, allowing the melt front to approach more closely. On the other hand, the Can B melt front temperature cooled after the Can C rupture. In this case it appears the gas from Can C cooled the melt front near Can B. A plot of Type C

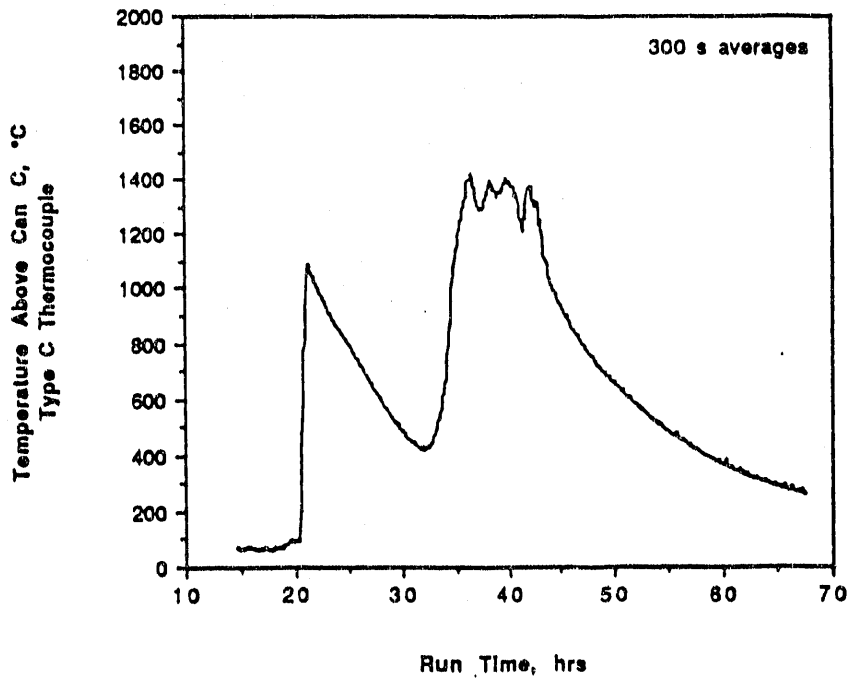

FIGURE 4.21. Type C Thermocouples Data

thermocouple temperature above Can C is shown for the entire run in Figure 4.22. It shows a maximum melt temperature of 1400°C.

The temperatures inside the cans remained relatively cool and constant prior to rupture, which indicated that vaporization was taking place in the can. The can pressurized, began to leak, and the vaporization of the liquid in the can (water with some volatile hydrocarbon) kept the can temperature cool. Since temperatures inside Cans A and C were relatively cool prior to rupture, some unvolatilized liquid was still in the cans at that time. When the cans ruptured, this liquid volatilized and was a portion of the release to the hood.

The leakage from the cans also appeared to cool the melt front temperature. As can be seen in Figures 4.14 and 4.18, the melt front appeared to be cooled during depressurization and the bursting of Cans A and C.

All the cans went through a series of depressurizations and repressurizations. There are several potential explanations for these cycles, including plugging of the can leak by particulates or glass, changes in the rate of

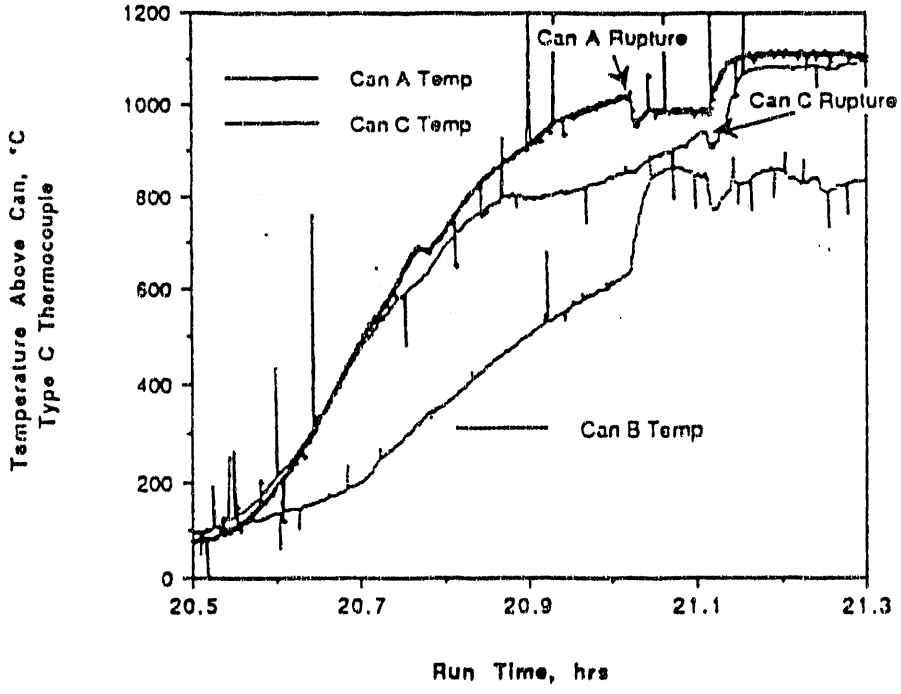

NOTE: Due to an improperly sized signal conditioner, plots of temperature show occasional random spikes up and down.

FIGURE 4.22. Type C Thermocouples Above Canisters

heat transfer from the melt, or changes in the composition of the cans as the vapors leak from the can.

The latter is the most likely since, in the case of the first two explanations, the temperature inside the can should increase with the pressure. This does not appear to have happened in several cases, especially in the first pressurization. However, the local environment around the thermocouple could have prevented seeing the change.

Changes in the composition of the vapors could explain large changes in pressures with comparatively small changes in internal temperature. For example, the initial pressure spike may have been due to the vapor pressure being exerted by both the volatile hydrocarbon (in this case, mainly CCl_4) and water. As vapor leaked from the can, the more volatile CCl_4 was preferentially released. If enough CCl_4 was released, it no longer exerted its full vapor pressure and the pressure inside the can decreased. Further leakage would mainly occur at the vapor pressure of water until a further composition change occurred (e.g., a solubility limit was reached or decomposition of a

compound occurred). The complexity of the mixture made this behavior difficult to predict; however, the later pressure spikes appeared higher than what would have been predicted for water alone at the temperatures in the can (e.g., the vapor pressure of water at 150°C is 374 kPag, and at 125°C, 131 kPag.

What are the rates of canister depressurization and melt encapsulation, and the relationships between each rate?

A comparison between Cans A, B, C, and D can be made to help answer this question (Figure 4.23). Cans A and C depressurized very rapidly (burst) within the 0.5-s sampling time of the data acquisition system (Figures 4.3 and 4.4). Cans B and D depressurized more slowly (see Figures 4.17 and 4.20). In all cases, melt encapsulation proceeded fairly rapidly once the canister had fully depressurized. However, because Cans B and D depressurized more slowly, their encapsulation was delayed. This is not surprising since the vaporization of the water in the sludge can provide a mechanism to cool the can (and

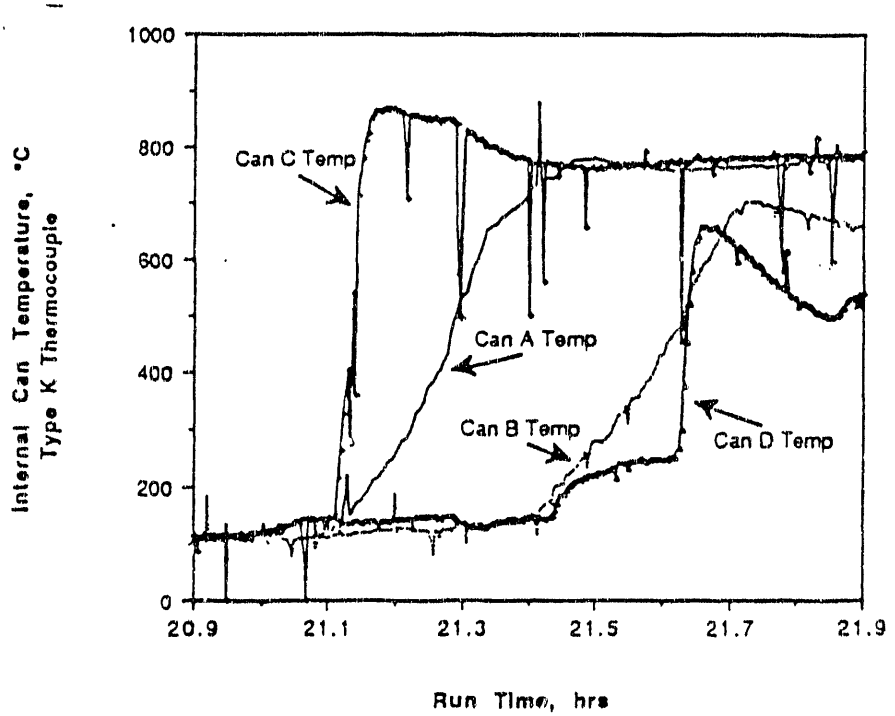

FIGURE 4.23. Canister Internal Temperatures

the melt above), hence slowing encapsulation. It also should be noted that power was shut off prior to the rupture of Cans A and C, which affected the rate of encapsulation.

Another interesting phenomenon can be observed from the temperature data in the cans. Plots of 5-min average temperature data from the instrumented cans are given in Figures 4.24 through 4.29. The temperatures for virtually all the cans spiked at 600 to 800°C and decreased before rising again. The spike was likely due to endothermic chemical changes occurring prior to melt encapsulation (e.g., release of chemically bound water). This temperature change did not affect the can pressure. (The cans had fully depressurized by this time.)

What is the product quality of the vitrified block and surrounding soils resulting from ISV processing?

Results for the TCLP inorganic materials in the glass block are given in Table 4.4. In general, these results are well below detection limits or

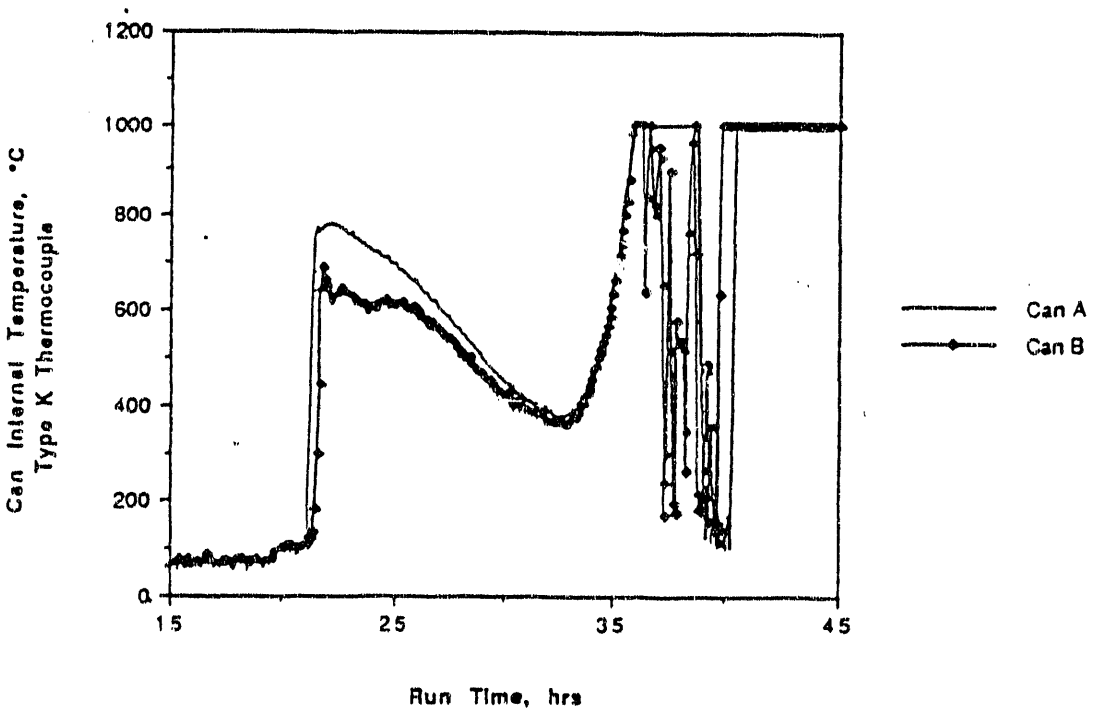

FIGURE 4.24. Internal Temperature for Cans A and B

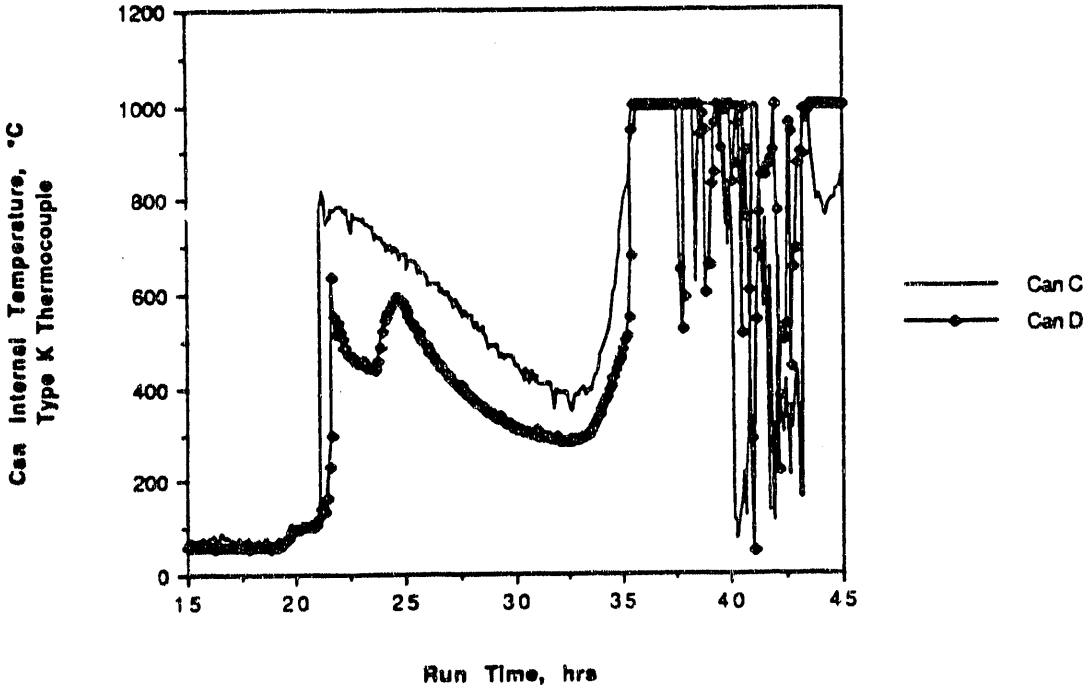

FIGURE 4.25. Internal Temperature for Cans C and D

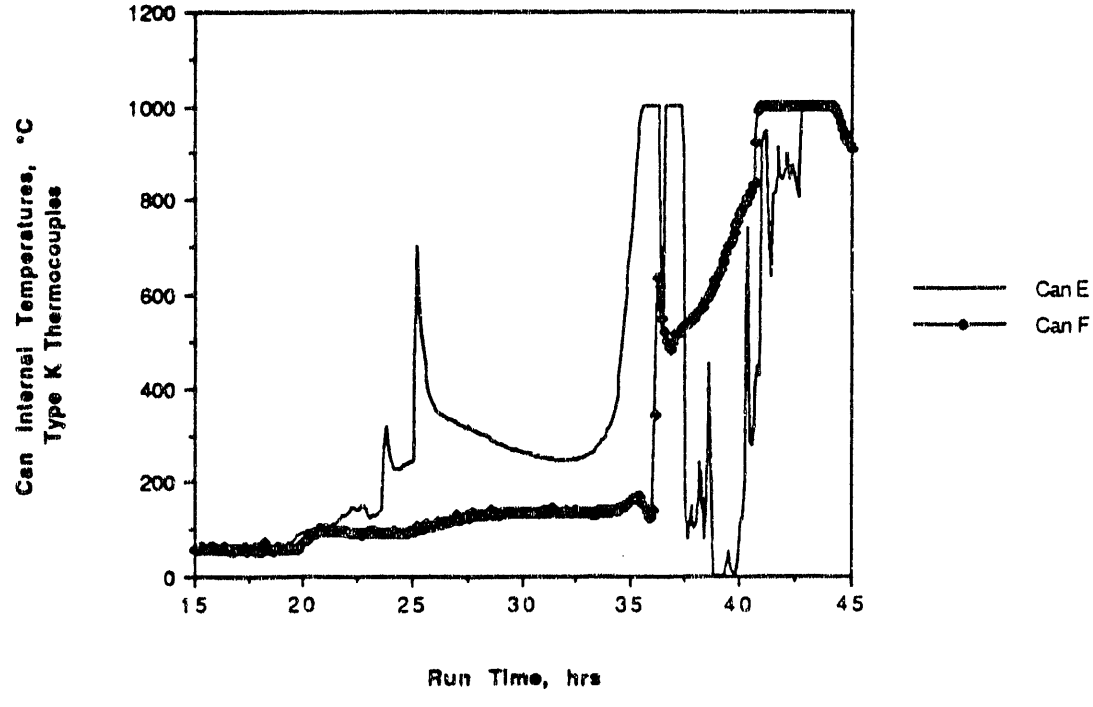

FIGURE 4.26. Internal Temperature for Cans E and F

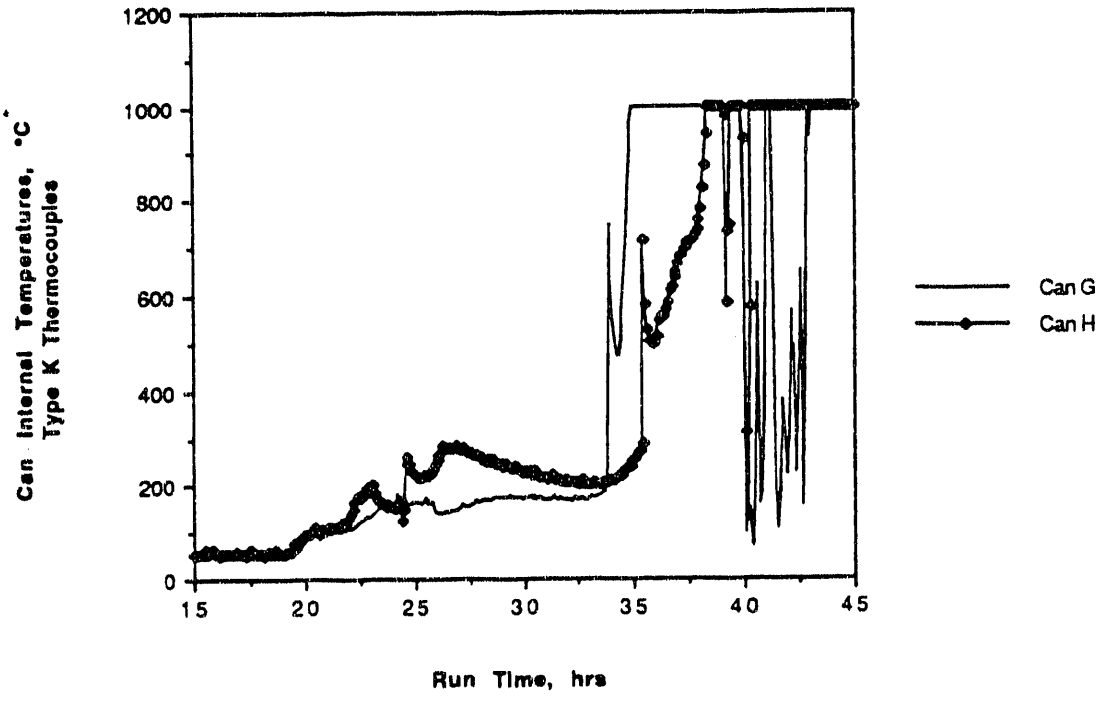

FIGURE 4.27. Internal Temperature for Cans G and H

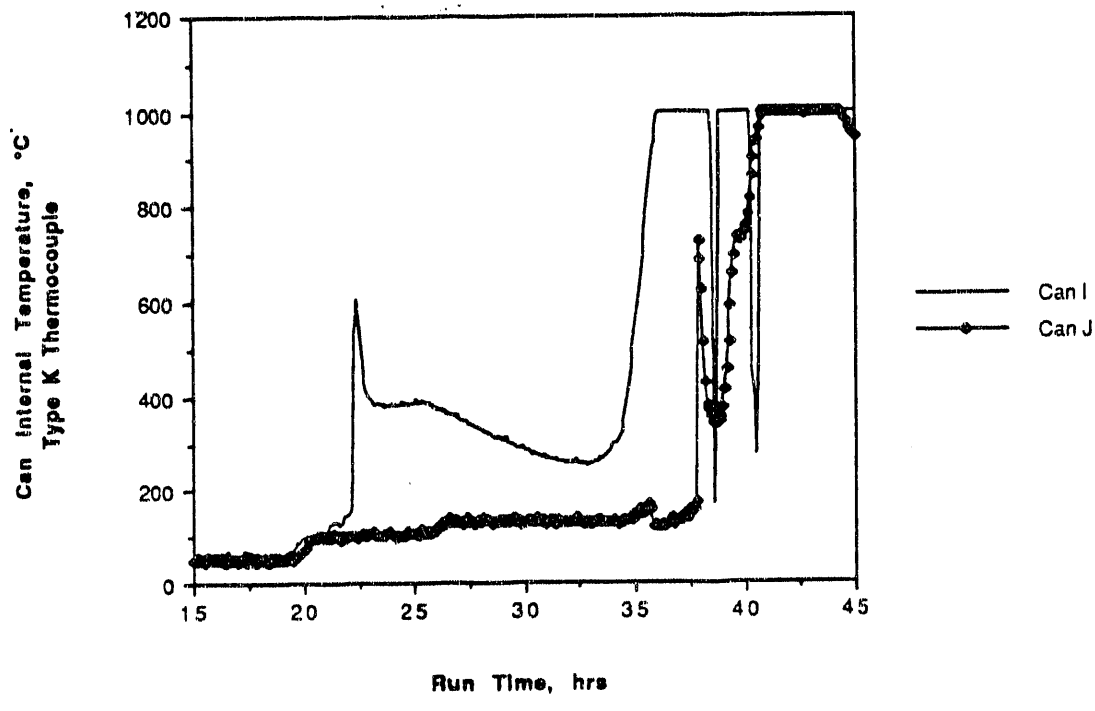

FIGURE 4.28. Internal Temperature for Cans I and J

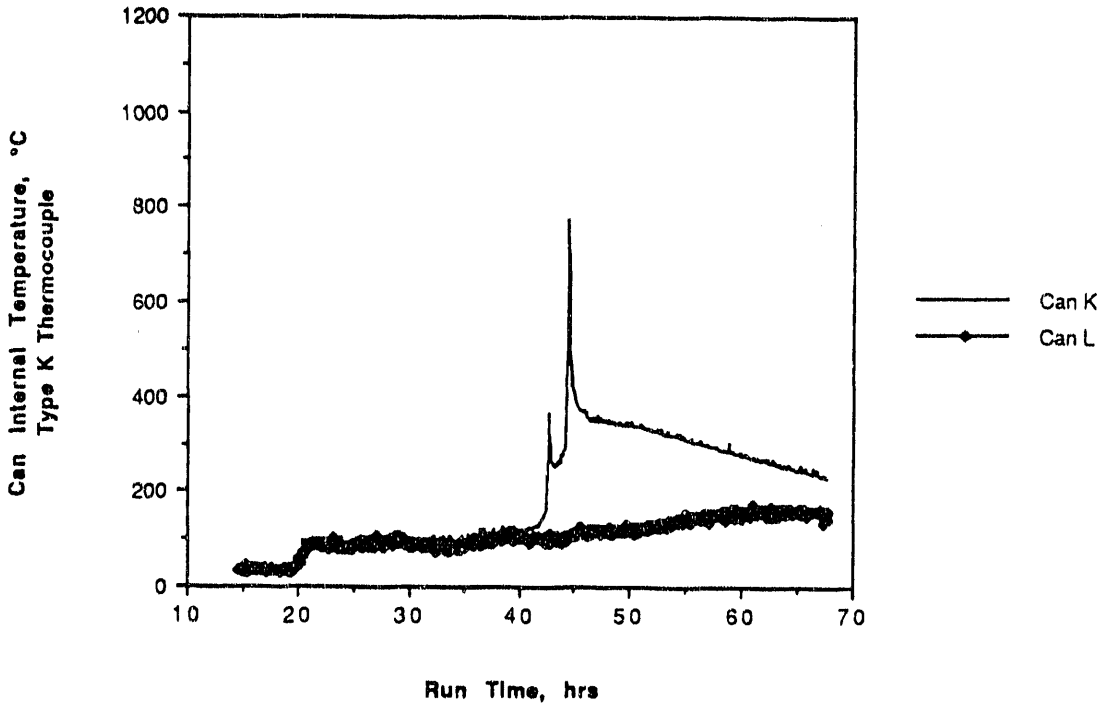

FIGURE 4.29. Internal Temperature for Cans K and L

several orders of magnitude below acceptable limits; therefore, the vitrified block can be considered nonhazardous.

The GC/MS and TCLP ZHE results of volatile organics in soil samples are given in Table 4.5. These samples were collected at the 350°C, 150°C, 100°C, and 50°C isotherms on both sides of the vitrified block (can side and soil

TABEL 4.4. TCLP Results for the Vitrified Block, ppb

Sample	AG	As	Ba	Cd	Cr	Hg	Pb	Se
A	<15	<15	13	<4	<9	<0.10	<77	<15
B	<15	<15	14	<4	20	<0.10	<77	<15
B	<15	<15	14	<4	23	0.11	<77	<15
C	17	<15	13	<4	<9	0.12	<77	<15
D	<15	<15	14	<4	14	<0.10	<77	<15
TCLP Regulatory Limit	5,000	5,000	10,000	1,000	5,000	200	5,000	1,000

TABLE 4.5. Volatile Organics in Soils and Soil TCLP-ZHE

		Soil Organic Analysis (ppb)												
		Can Side				Soil Side				Below Melt				
Isotherm, °C		350	150	100	50	350	150	100	50	350	150	100	50	TCLP Regulatory Limit
Compound														
CCl_4	GC/MS	<5	<5	<5	<5	<5	<5	<5	<5	<5	<5	<5	<5	
(A)[a]	TCLP	(<5)	(<5)	(<5)	(<5)	(<5)	(<5)	(<5)	(<5)	(<5)	(<5)	(<5)	(<5)	500
PCE	GC/MS	15	<5	<5	<5	81	<5	<5	<5	168	<5	<5	<5	
(A)	TCLP	(<5)	(<5)	(<5)	(<5)	(<5)	(<5)	(<5)	(<5)	(34)	(<5)	(<5)	(<5)	700
TCA	GC/MS	30	<5	<5	<5	290	<5	<5	<5	174	<5	<5	<5	
(B)	TCLP	(<5)	(<5)	(<5)	(<5)	(18)	(<5)	(<5)	(<5)	(50)	(<5)	(18)	(<5)	N/A
TCE	GC/MS	56	<5	<5	<5	80	<5	<5	<5	459	<5	<5	<5	
(C)	TCLP	(<5)	(<5)	(<5)	(<5)	(<5)	(<5)	(<5)	(<5)	(118)	(<5)	(<5)	(<5)	500

[a]( ) = Canister series

side), as well as directly beneath the block.[a] The sample temperatures on the canister side, soil side, and below the melt are useful to compare relative thermal gradients and thermal symmetry with respect to the block. Organic compounds measured were TCA, TCE, PCE, and CCl_4. The values shown in Table 4.6 are averages from duplicate samples at each location. As stated earlier, CCl_4 and PCE were contained in the Series A canisters, TCA in the Series B canisters, and TCE in the Series C canisters. (See Figure 3.1 for the location of each series.)

Several observations can be made from these data concerning the distribution of organics around the melt. Based on GC/MS analyses of the surrounding soil samples, there were no measurable organics found at temperatures below the 350°C isotherm and no measurable CCl_4 was found in any soil sample. The only detectable concentrations in TCLP-ZHE tests were found in 350°C

(a) The isotherm locations were determined based on the maximum temperature readings experienced by the Type K thermocouples in the soil surrounding the vitrified block.

samples for TCA on the soil side and for TCA, TCE, and PCE below the vitrified block. Furthermore, the results of the TCLP-ZHE tests for the surrounding soils are well below the established regulatory limits. These data suggest that volatile organics were in large part either transported to the off-gas system or destroyed. This process probably included some pyrolysis and

TABLE 4.6. Net Trace Element Concentration in Soils

	Soil Trace Element Distribution (ppm)[a]											
	Can Side				Soil Side				Below Melt			
Isotherm, °C	350	150	100	50	350	150	100	50	350	150	100	50
Element[b]												
Dy(A)	1.3	0.4	0.3	0.1	0.6	0.7	1.2	0.2	0.3	0.4	0.8	0.2
Yb(B)	0.6	0.4	0.3	0.2	0.3	1.1	1.2	0.4	0.4	0.7	0.3	0.3
Nd(C)	143	5.9	2.7	1.9	5.3	5	8.7	2.2	2.4	4	2	0.4
Ce(D)	18.8	6.3	7.9	9.3	12.3	13	27.5	8	9.4	8.3	4.7	2.3
Hg(A)	135	41	6.1	2.1	9.6	5.6	4.2	0.2	0.3	7.1	0.3	0.2
H(TCLP)	0.001	0.14	0.3	0.003	0.003	0.003	0.002	<0.0001	<0.0001	0.001	<0.0001	<0.0001

[a] Concentration = posttest soil concentration - pretest soil average.
[b] ( ) = Canister series.

combustion during transport. These results for volatile organics are consistent with the results found in ES-INEL-4 (Shade et al. 1991), which also indicated that volatile organics do not tend to accumulate in soils.

The ICP/MS and TCLP values for Hg concentrations in soils are shown in Table 4.6. These values are mean values from duplicate samples. All Hg TCLP values are below the toxicity limit of 2.0 ppm except for one sample on the canister side at the 100°C isotherm. This value does not correspond with the highest Hg content soils (as measured by ICP/MS--see Table 4.6). A possible explanation for this is that the Hg at the 100°C isotherm may have remained in the oxide form. As discussed earlier, the canisters ruptured with significant force. This could easily have resulted in significant gas entrainment of particulate, including the mercuric oxide in the Series A canisters. In addition, the test canisters were arranged in a line (not randomly), such that entrainment would be enhanced (see Figure 3.2). This would explain the

greater amount of Hg on the canister side versus the soil side. The mercuric oxide closer to the melt may have been exposed to sufficient heat and reducing conditions from the organics in the sludge to convert to Hg metal. The metal form may be less likely to leach in the TCLP procedure than the oxide form. Given the uncertainty in the analyses (the ICP/MS results have been designated as for indication only), additional study is required to evaluate the effect of pressurized releases on Hg transport. Further work should concentrate on ruptures more likely to be representative of the INEL SDA.

The distributions of Ce, Nd, Dy, and Yb in the soils after the test are also given in Table 4.6. For each isotherm, these samples were obtained at approximately the same location as the organic soil samples. The concentration values for the elements in Table 4.6 represent net values that were obtained by subtracting the mean values of four analyses of pretest soil samples from the mean of two posttest samples. The net concentrations in Table 4.6 are thus intended to represent trace elements supplied by the spike sludge.

Part of these net concentrations may be the result of the ISV process itself, which could affect the bulk density of the surrounding soils by changing the moisture and organic content and causing soil mineral reactions. Of all the trace elements, only Ce and Nd had natural pretest soil values above 1 to 3 ppm. The mean pretest soil concentration of Ce was 27 ppm (Standard deviation = 2.32), and for Nd it was 17 ppm (standard deviation = 1.13). Initial Hg values were about 0.06 ppm. The variance associated with duplicate posttest soil analyses was generally larger than those for the pretest soil based on four samples.

As shown in Table 4.6, most of the Dy and Yb did not migrate into the soils, but was largely assimilated into the melt, and only a very small portion was entrained into the off-gas system. The low amounts of Dy and Yb in the soils, on the order of 1 ppm, did not exhibit any apparent temperature dependence, indicating little lateral movement. Also, the concentrations were generally symmetrical with respect to the glass block. This suggests that most of the nonvolatile components of the Series A and B canisters were

assimilated in the melt. This is consistent with the observation that nearly all of these series of cans were assimilated.

The net concentration of both Nd and Ce are higher in the soils around the vitrified block than Dy and Yb. Since Ce was contained in the D series canisters, and post test observation indicated that these canisters had not been breached, it is likely that the higher concentration of Ce was a result of either a change in the bulk density of the soil or a systematic error in the analyses. However, assuming none of the Ce was lost from the D series canisters, Ce can be used as a reference to determine the distribution of Nd in the soil around the melt. To do this, the Ce/Nd ratio is calculated for each location in the soil. These ratios are given in Table 4.7.

TABLE 4.7. Ce/Nd Concentration Ratios in Soils[a]

	Isotherm, °C			
	350	150	100	50
Soil Side	1.7	1.8	2.1	1.8
Below Melt	1.9	1.7	1.7	1.7
Can Side	0.3	1.5	1.8	1.9

(a) Uncorrected for initial pretest soil concentrations.

Pretest soil concentration ratio = 1.6 +/- 0.2

On the soil side and in the sample area below the melt, the Ce/Nd ratios are similar to those in the original, pretest soil. Thus the major source of Nd in these areas is like the soil itself. (However, these ratios are all some degree higher than the pretest ratio. This appears to indicate a potential systematic difference in the analyses pre and post test.) On the can side, the Ce/Nd ratio at the 350 °C isotherm is significantly less than the pretest soil and the ratio at the 150 °C isotherm is potentially less. This indicates Nd from the C series canisters was present in these areas. Post test observations support this potential. Several of the C series canisters were ruptured and, hence, were likely to have distributed Nd to the soil.

Analysis of the glass block and the pretest soil were used to determine what degree the various trace elements from the canisters were incorporated into the glass block. The results of this analysis are given in Table 4.8. The estimate of the initial mass in the soils is based on the assumption that all the Ce in the glass is from the soil. This assumption does give an unrealistically high densification factor (approximately 3), and is the likely reason for the overestimation of the Dy. However, the relative amounts of incorporation appear feasible. These show that very little of the Nd (from the C series canisters) was incorporated into the melt, 60 to 70% of the Yb (B series) was incorporated, and essentially all of the Dy (A series) was incorporated.

TABLE 4.8. Trace Element Content of Vitrified Block

	Dy(A)	Yb(B)	Nd(D)	Ce(D)	Ce/Nd
Pretest Soil, ppm	2.28	0.81	16.9	27.0	1.6
Glass Block, ppm	157.6	234.2	52.1	78.8	1.51
Est. Initial Mass in Soil, g[(a)]	1.5	0.5	11.1	17.7[(a)]	
Initial Mass in Cans, g	28.6	76.0	57.1	84.2	1.47
Total Mass in Glass, g	35.4	52.5	11.7	17.7[(a)]	
Percent of Can Mass Incorporated into Glass	118	68	1	0	

(a) Initial mass in soil estimated assuming all Ce in glass was from posttest soil.

Does the presence of a sealed drum layer enhance the thermal transport of organics and semivolatile inorganics away from the advancing melt front?

The soil sampling results (see Table 4.5) can also be used to provide an indication of the effect of the canister layer on the transport of volatile organics. Interestingly, it appears that the concentrations of TCA, TCE, and PCE are slightly higher below the melt and on the soil side than on the canister side. (The results below the melt and on the soil side are not statistically different due to the high standard deviation of the duplicate

analyses.) The difference might be explained by recalling the force with which the canisters ruptured. Significant entrainment of vapor could have occurred (e.g., TCE, which was contained in the Series C canisters, was found on the soil side, the opposite side from the location of the Series C canisters). The vapor likely traveled until it was stopped by the lower permeable region (e.g., the soil). Since the driving force for recovery back into off gas would be less than the force that initially entrained the vapor, it would take some time for this recovery to occur. On the canister side, higher permeability and potential localized heating may have allowed the materials to be removed more easily. In addition, canisters were heard rupturing after the power was turned off, so the compounds in these canisters (either TCA in Series B or TCE in Series C) may not have had sufficient time to transport to the off-gas system. Since none of the compounds are found outside the 350°C isotherm, and their boiling points are low (TCA is 74.1°C; TCE is 87.2°C; PCE is 120.8°C), it appears that they were not being thermally driven from the melt.

Interestingly, the GC/MS soil results (see Table 4.5) show that PCE was present in the surrounding soils, but that CCl_4 was not. Both of these contaminants were present in the Series A canisters, which were totally encapsulated by the melt. The presence of PCE in the surrounding soils suggests that during the rupture of the canisters, PCE may have been driven outward, then, because of its high boiling point, did not have sufficient time to be recovered back to the off-gas system.

The amount of Hg is greater on the canister side than on the soil side. As discussed earlier, this is likely due to gas entrainment of particulate or vapor from the force of the rupturing canisters. The higher value on the canister side is likely caused by the greater permeability on the canister side of the melt (since the test canisters were arranged in a line). The Hg, then, was not sufficiently volatile to be recovered back into the off-gas system. If the transport was strictly a thermal one, Hg would not be expected to be found at isotherms less than approximately 350°C (the condensation point of Hg).

How is the entrainment of nonvolatile particulates related to the approach angle of the advancing melt front?

The amount of lanthanide tracers and mercury collected on off-gas system components is given in Table 4.9. Dysprosium and Yb values are slightly lower than Ce and Nd, which is consistent with observations that a large fraction of Dy and Yb were retained by the glass. Slightly more of the Yb than Dy was present on the filter and insulation, which is consistent with the can layer geometry and the higher melt approach angle for Yb cans than Dy cans. Nd is

TABLE 4.9. Trace Element Concentration in Off-Gas System, ppm

Component	Hg	Dy	Yb	Nd	Ce
Impinger Solution	0.32	DL	DL	DL	0.01
Impinger Filter	29.4	0.35	2.54	3.67	0.83
Cover Insulation	33.6	0.38	0.95	9.8	1.06

higher than Ce in both the filter and insulation, which is also consistent with the observation that some of the Series C cans ruptured, but none of the Series D cans ruptured.

Does the pressurized release of gas-generating materials (such as water, volatile organics, and nitrates) from sealed carbon steel containers increase the volatility and entrainment of hazardous or radioactive materials to the off-gas system? Would this result in incomplete organic combustion above the melt?

The concentration in the SUMA cans is given in Table 4.10. SUMA Can 117 was opened only at the peak of a pressurization. SUMA Can 556 was opened for the duration of the test operation, and SUMA Can 555 was opened during posttest cool down.

It is difficult to determine from these data the relative increase in volatility or entrainment of hazardous materials due to the pressurized release of gases. Unfortunately, these data are compromised because off-gas flow rates were adjusted during the test due to pressurization. In order to truly answer this question, a continuous analyzer must be used or a greater

series of batch samples must be taken. For the same reasons, organic combustion has not been evaluated. Hence, this test objective was not met.

Certain information, however, can be gained from these data. The dominance of CCl_4 and PCE in Can 117 suggests the peak pressurization was largely generated by ruptures of Series A cans (as indicated by the pressurizations of Cans A and C discussed in the previous section), although the presence of TCE and small amounts of TCA indicate some Series B and C cans may have leaked. Also, the high amount of carbon dioxide in this can indicates an amount of

TABLE 4.10. Air and Volatile Organics in SUMA Cans

Can No.	CO_2 vol%	O_2%	N_2%	CCl_4	PCE	TCA µg/cum	TCE
556	1.6	21	77	6600	6800	35000	32000
555	0.7	21	78	190	440	1700	63000
117	9.1	18	73	82000	56000	730	18000

combustion occurred. The amount of CO_2 is too large compared with the organics available and may also include CO_2 from electrode oxidation and soil decomposition.

At the end of the test, results showed that gases collected in SUMA Can 555 consisted largely of TCE, indicating some of the Series C canisters ruptured or leaked. There was also a late can rupture, probably a Series C can, after the melt was shut down. SUMA Can 556 was open during the duration of the test and thus, to a degree, represents a composite of gases generated.

5.0 REFERENCES

Buelt, J. L., Timmerman, C. L., Oma, K. H., Fitzpatrick, V. F., and Carter, J. G. 1987. In Situ Vitrification of Transuranic Waste: An Updated Systems Evaluation and Applications Assessment. PNL-4800 Suppl. 1, Pacific Northwest Laboratory, Richland, Washington.

Perry, R. H., and C. H. Chilton. 1973. Chemical Engineers Handbook, Fifth Edition. McGraw-Hill, New York.

Shade, J. W., R. K. Farnsworth, J. S. Tixier, and B. L. Charboneau. 1991. Engineering-Scale Test 4: In Situ Vitrification of Toxic Metals and Volatile Organics Buried in INEL Soils. PNL-7611, Pacific Northwest Laboratory, Richland, Washington.

Wierman, T. E. 1990. Field Test Siting and Source Term. EDF BWP-ISV-024, EG&G Idaho, Inc., Idaho Falls, Idaho.

NIOSH. 1990. Pocket Guide to Chemical Hazards. National Institute of Occupational Safety and Health, U.S. Department of Health and Human Services.

DISTRIBUTION

No. of Copies

OFFSITE

12 DOE/Office of Scientific and Technical Information

21 DOE Office of Environmental Restoration and Waste Management
Trevion II Building
Germantown, MD 20874
ATTN: W. W. Alexander
T. D. Anderson
J. E. Baublitz
D. L. Biancasino
J. O. Boda
J. Coleman
S. P. Cowan
J. J. Fiore
C. W. Frank
K. O. Hain
J. M. Lankford
J. C. Lehr
S. C. Lein
J. E. Lytle
S. A. Mann
S. M. Prestwich
M. Shupe
C. H. Sink
L. H. Taylor
H. F. Walter
R. P. Whifield

2 DOE Albuquerque Operations Office
P.O. Box 5400
Albuquerque, NM 87115
ATTN: P. A. Saxman
D. H. Bandy

W. Holman
DOE San Francisco Field Office
1333 Broadway
Oakland, CA 94612

No. of Copies

J. Haugen
DOE Chicago Field Office
9800 South Cass Avenue
Argonne, IL 60439

J. Hall
DOE Nevada Field Office
P.O. Box 98518
Las Vegas, NV 89193-8518

R. Tyler
DOE Rocky Flats Office
DOE Building 116
Golden, CO 80401-0928

S. Ketola
DOE West Valley Project
P.O. Box 191
West Valley, NY 14171

W. Fitch
DOE Idaho Operations Office
785 DOE Place
Idaho Falls, ID 83402

M. O'Rear
DOE Savannah River Operations Office
P.O. Box A
Aiken, SC 29801

4 DOE Oak Ridge Office
P.O. Box 2001
Oak Ridge, TN 37831
ATTN: J. Moore (2)
J. Sweeney (2)

3 Battelle Memorial Institute
505 King Avenue
Columbus, OH 43201
ATTN: W. A. Carbeiner
R. A. Nathan
Technical Library

No. of Copies

Jesse L. Yow, Jr.
Lawrence Livermore National Laboratory
7000 East Avenue
Livermore, CA 94550

M. A. H. Reimus
Los Alamos National Laboratory
P.O. Box 1663
Los Alamos, NM 87545

J. Koger
Martin Marietta Energy Systems
P.O. Box 2009
Oak Ridge, TN 37831-8097

P. T. Owen
Martin Marietta Energy Systems
Oak Ridge, TN 37831-7256

8 Oak Ridge National Laboratory
P.O. Box Y
Oak Ridge, TN 37830
ATTN: G. K. Jacobs (4)
M. Naney (2)
B. P. Spalding (2)

K. Nuhfer
Westinghouse Materials Co. of Ohio
P.O. Box 398704
Cincinnati, Oh 45239-8704

5 Sandia Laboratories
P.O. Box 5800
Albuquerque, NM 87185
ATTN: D. Berry
R. Knowlton
J. Phelan
L. D. Tyler
Technical Library

No. of Copies

4 EG&G Idaho
P.O. Box 1625
Idaho Falls, ID 83415
ATTN: S. K. Merrill
D. F. Nickelson
R. R. Stiger
S. Stiger

L. Rogers
EG&G Energy Measurements, Inc.
P.O. Box 1912, MS RSL-11
Las Vegas, NV 89125

J. R. Berreth
Westinghouse Idaho Nuclear Co., Inc.
P.O. Box 4000
Idaho Falls, OD 93401

B. Haas
Ames Laboratory
7 Spedding Hall
Iowa State University
Ames, IA 50011

6 Westinghouse Savannah River Company
P.O. Box 616
Aiken, SC 29801
ATTN: J. S. Haselow
C. M. Jantzen
M. J. Plodinec
J. F. Sproull
J. L. Steele
T. Walton

J. M. Pope
West Valley Nuclear Services Company
P.O. Box 191
West Valley, NY 14171

No. of Copies

4 Geosafe Corporation
2000 Logston Boulevard
Richland, WA 99352
ATTN: C. L. Timmerman (2)
B. E. Campbell
J. E. Hanson

ONSITE

13 DOE Richland Field Office

E. A. Bracken, A6-95
K. W. Bracken, A5-22
R. P. Carter, A5-21
P. K. Clark, A6-80
P. F. Dunigan, A6-95
J. K. Erickson, A5-19
R. D. Freeburg, A5-19
M. J. Furman, A6-80
R. E. Gerton, A6-80
J. D. Goodenough, A5-22
J. M. Hennig, A5-21
R. D. Izatt, A6-95
J. J. Sutey, A5-90

13 Westinghouse Hanford Company

W. C. Alaconis, L4-92
H. Babad, B3-68
J. D. Berger, L0-18
J. W. Cammann, H4-54
K. R. Fecht, H4-56
R. E. Lerch, B2-35
H. E. McGuire, B2-35
J. W. Shade, R4-03
D. A. Turner, R1-10
D. D. Wodrich, R1-48
R. D. Wojtasek, B2-15
B. A. Wolfe, L5-61
R. L. Gilchrist, L5-63

35 Pacific Northwest Laboratory

L. Ballou, P7-18
T. M. Bergsman, P7-41 (5)
W. F. Bonner, P7-44

No. of Copies

J. L. Buelt, P7-41
H. C. Burkholder, P7-41
C. C. Chapman, P7-41
T. T. Claudson, K1-66
W. O. Heath, P7-41
W. L. Kuhn, P8-38
P. A. Lowery, K7-15
J. Luey, P7-34 (5)
J. L. McElroy, P7-46
M. E. Peterson, P7-41
T. D. Powell, P7-34
M. R. Shay, K6-25
S. C. Slate, K1-25
S. L. Stein, PNWD
L. E. Thompson, P7-34
J. S. Tixier, P7-34
C. L. Widrig, K1-25
S. L. Woosley, P7-34
Publishing Coordination
Technical Report Files (5)

DATE
FILMED
8/31/92